

ARTICLE OPEN



Active R-RAS2/TC21 prevents cell cycle arrest and morphological alterations in mouse embryonic fibroblasts lacking RAS proteins

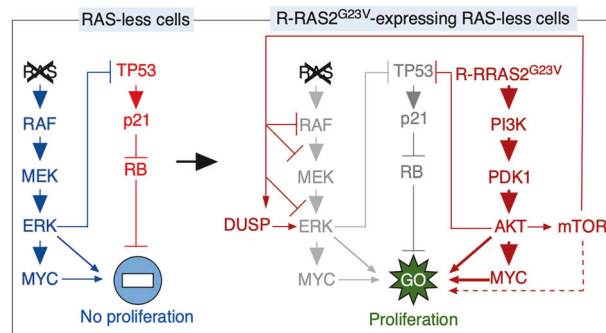
Isabel Fernández-Pisonero ^{1,2,3}, L. Francisco Lorenzo-Martín ^{1,2,3,6}, Mattias Drosten ^{1,2,3}, Eugenio Santos ^{1,2,3}, Mariano Barbacid ^{3,4}, Balbino Alarcón ⁵ and Xosé R. Bustelo ^{1,2,3}✉

© The Author(s) 2025

R-RAS2/TC21, a member of the R-RAS subfamily of GTP-binding proteins, shares structural and signaling properties with the RAS subfamily proteins H-, K-, and N-RAS. However, little information is available regarding its role in normal cells and the level of functional redundancy with R-RAS and classical RAS proteins. In this work, we used loss and gain-of-function approaches to assess these issues in mouse embryonic fibroblasts (MEFs). Using primary MEFs from *Rras2*^{-/-}, *Rras*^{-/-} or *Rras*^{-/-}; *Rras2*^{-/-} embryos, we show here that endogenous R-RAS2/TC21 is required for activation of the phosphatidylinositol 3 kinase (PI3K)–AKT axis, the proliferation, and the adhesion properties of these cells. Endogenous R-RAS does not influence any of these cell parameters. We also show that the depletion of R-RAS2/TC21 worsens the proliferative and morphological defects elicited by the combined loss of H-, K- and N-RAS proteins in MEFs. Conversely, the ectopic expression of an active version of R-RAS2/TC21, but not of R-RAS, overcomes such defects. This rescue activity involves the inhibition of the tumor suppressor TP53 and is PI3K-, mTORC-, and MEK/ERK-dependent. These results indicate that R-RAS2/TC21, R-RAS, and RAS subfamily GTPases play different roles in MEFs. They also show that R-RAS2 provides subsidiary signals that are essential for the short-term proliferation and long-term viability of MEFs lacking RAS signaling.

Oncogene (2025) 44:1905–1921; <https://doi.org/10.1038/s41388-025-03367-3>

Graphical Abstract



INTRODUCTION

R-RAS2, also known as teratocarcinoma clone 21 or TC21 [1], is a GTP hydrolase (GTPase) that belongs to the R-RAS subfamily [2]. Recently, gain-of-function mutations in the *RRAS2* gene have been found with low frequency in human tumors [3–7] and in Noonan syndrome [8–10], a germline disease generally associated with genetic alterations in elements of the RAS signaling pathway [11, 12]. Evidence suggests that *RRAS2* mutations play a significant

pathological role in tumors. For example, we recently demonstrated, using an inducible knock-in mouse model, that the somatic expression of one of the hot-spot mutations found in the *RRAS2* gene in pan-cancer data (Q72L) behaves as a bona fide oncogenic driver in a variety of solid and hematopoietic tumors [3]. This mutation is analogous to the oncogenic Q61L mutation found in RAS proteins (the number of amino acids in the primary structure of R-RAS2 is shifted +11 positions relative to those found

¹Molecular Mechanisms of Cancer Program, Centro de Investigación del Cáncer, CSIC and Universidad de Salamanca, Salamanca, Spain. ²Instituto de Biología Molecular y Celular del Cáncer, CSIC and Universidad de Salamanca, Salamanca, Spain. ³Centro de Investigación Biomédica en Red de Cáncer (CIBERONC), Instituto de Salud Carlos III, Madrid, Spain. ⁴Centro Nacional de Investigaciones Oncológicas (CNIO), Madrid, Spain. ⁵Centro de Biología Molecular Severo Ochoa, CSIC and Universidad Autónoma de Madrid, Madrid, Spain. ⁶Present address: Laboratory of Stem Cell Bioengineering, Institute of Bioengineering, School of Life Sciences and School of Engineering, École Polytechnique Fédérale de Lausanne, Lausanne, Switzerland. ✉email: xbustelo@usal.es

Received: 8 May 2024 Revised: 26 February 2025 Accepted: 20 March 2025
Published online: 31 March 2025

in RAS proteins due to the presence of an 11 amino acid long sequence located at the R-RAS2 N-terminus). We also reported that the elimination of endogenous R-RAS2^{Q72L} alters the growth of human cancer cell lines both in cell culture and in orthotopic transplantation experiments [7]. Although the role of *RRAS2* mutations in Noonan syndrome has not yet been modelled in mice, zebrafish studies suggest a causal role for *RRAS2* mutations in this disease [4]. Transgenic mouse models have further shown that the overexpression of wild-type R-RAS2 leads to B cell leukemogenesis and breast cancer [5, 6].

Despite these findings, the level of functional redundancy of R-RAS2/TC21 with other members of the R-RAS (R-RAS, M-RAS) subfamily and the RAS subfamily (H-RAS, K-RAS, N-RAS, from now on referred to as RAS proteins) is not yet understood well. Endogenous R-RAS2/TC21 and R-RAS share similar subcellular location at focal adhesions and a similar spectrum of both positive and negative regulators [7–9]. However, gain-of-function versions of R-RAS2 display much higher levels of transforming activity than the analogous R-RAS mutants when ectopically expressed in immortalized cell lines [7, 10–14]. In fact, the oncogenic activity of R-RAS mutants is debatable depending on the study involved [14, 15]. This suggests that their functions may not be entirely convergent.

The functional overlap between R-RAS2/TC21 and RAS proteins also remains unclear. On the one hand, it has been shown that R-RAS2/TC21 and RAS proteins can engage similar downstream effectors, including RAL GDP dissociation inhibitor, RAF family kinases, and PI3Kα [9, 11, 12, 15–19]. Consequently, gain-of-function mutations of R-RAS2/TC21 can activate the RAF–MEK–ERK–RSK and PI3Kα–AKT–mTORC1 pathways in cells [9, 11, 12, 15–19]. It is worth noting, however, that the activation of the ERK pathway by R-RAS2/TC21 is cell type-dependent [3, 7, 20–23]. In line with this signaling similarity, R-RAS2/TC21 is the only known GTPase whose gain-of-function mutant versions have transforming activities comparable to classical RAS proteins [10, 11]. However, on the other hand, evidence indicates that R-RAS2/TC21 and RAS proteins are not fully functionally redundant. For example, the gain-of-function R-RAS2^{Q72L} mutant protein induces tumor types in mice that overlap with, but are not identical to, those found in analogous mouse models for RAS proteins [3]. The subcellular localization of endogenous R-RAS2/TC21 also differs from classical RAS proteins [7]. A significant indication of this lack of functional redundancy is the observation that the ectopic expression of the gain-of-function R-RAS2^{G23V} protein (bearing a mutation analogous to the G12V mutation found in RAS proteins) fails to rescue the morphological and proliferative defects present in MEFs lacking the three RAS proteins [24]. In this model, the deletion of the three RAS proteins induces cell cycle arrest due to the loss of an ERK-dependent mechanism that inhibits suppressor protein TP53 in normal cells (a scheme for this pathway can be found in Supplementary Fig. 8; points a, b1, and b2) [25, 26].

In this study, we decided to use primary and immortalized MEF models to investigate the functional redundancy of R-RAS2/TC21 with R-RAS and classical RAS proteins using knockout, knockdown and ectopic expression strategies. Our results indicate that: (i) endogenous R-RAS2/TC21 and R-RAS do not exhibit functional overlap in the biological parameters tested in this study in MEFs; (ii) endogenous R-RAS2/TC21 plays supportive roles to the signaling of RAS subfamily proteins in MEFs. These roles are unmasked when H-, K- and N-RAS are eliminated in these cells; and (iii) the ectopic expression of an active R-RAS2/TC21 mutant version provides signals that overcome the proliferative and morphological defects elicited by the RAS deficiency in MEFs, although it fails to do so in the case of cells lacking basal MEK or ERK activity. These findings highlight the important roles of R-RAS2/TC21 in the signaling, proliferative, and adhesion properties of MEFs.

RESULTS

Signaling of endogenous R-RAS2/TC21 is important for primary MEFs

We obtained primary MEFs from wild-type mice, single *Rras*^{-/-}, single *Rras2*^{-/-}, and double *Rras*^{-/-}; *Rras2*^{-/-} mice to analyze the impact of R-RAS and R-RAS2/TC21 on the proliferation and signaling properties of this cell type. Elimination of R-RAS2/TC21, either alone or in combination with R-RAS (Fig. 1A), caused similar reductions in the proliferation rates of primary MEFs (Fig. 1B). The single elimination of R-RAS (Fig. 1A) did not result in a statistically significant reduction in proliferation rates (Fig. 1B), suggesting that this GTPases does not play any major role in this process in MEFs. Further experiments revealed that the R-RAS2/TC21 deficiency also led to decreased phosphorylation of PDK1-dependent (Fig. 1C, upper panel) and mTORC2-dependent (Fig. 1C, second panel from top) phosphosites in AKT after stimulation of serum-starved MEFs with epidermal growth factor (EGF) (statistics in Fig. 1D, E). These defects were associated with reduced phosphorylation of S6K (Fig. 1C, third panel from top), a downstream signaling element of the PI3K–AKT–mTORC1 pathway. However, the lack of endogenous R-RAS2 did not affect ERK phosphorylation (Fig. 1C, fourth panel from top; statistics in Fig. 1F). Similar results were obtained in MEFs lacking both R-RAS2 and R-RAS (Fig. 1G, statistics in Fig. 1D–F), while the single loss of R-RAS did not alter AKT or ERK phosphorylation levels in primary MEFs (Fig. 1H). These results demonstrate that R-RAS2 and R-RAS are not functionally redundant in the parameters examined in MEFs. They also indicate that R-RAS2 is important for the activation of the PI3K–AKT pathway even in MEFs that normally express H-, K- and N-RAS.

Given the focal adhesion localization of endogenous R-RAS2 in fibrosarcoma cells and other cell types [7], we next examined the effect of the loss of R-RAS2 on MEF adhesion and wound healing properties. As shown in Fig. 2A, B, primary *Rras2*^{-/-} MEFs showed a reduction in adhesion compared to control MEFs. However, once adhered to the plates, the *Rras2*^{-/-} MEFs did not show adhesion differences from controls in culture (Fig. 2C). Primary *Rras2*^{-/-} MEFs also exhibited defects in wound healing compared to wild-type MEFs (Fig. 2D, E). Taken together, these results indicate that endogenous R-RAS2/TC21 is important for the activation of the PI3K–AKT axis as well as for regulating the proliferation, cell adhesion, and wound-healing properties of primary MEFs.

Endogenous R-RAS2/TC21 affects the proliferation and viability of RAS-less MEFs

Next, we investigated the role of endogenous R-RAS2 in MEFs lacking expression of the three classical RAS proteins. To this end, we used the previously described *Hras*^{-/-}; *Kras*^{LoxP/LoxP}; *Nras*^{-/-}; *CreER*^{T2} MEF cell line (designated hereafter as DU cells) [24] that was further manipulated to create two independent knockdown variants with short hairpin RNAs (shRNAs) targeting the *Rras2* mRNA (sh*Rras2*#89 and #478). As control, we generated DU cells transduced with an empty lentiviral vector (pLKO). Western blot analyses confirmed that these two *Rras2* shRNAs reduced the expression of endogenous R-RAS2 (Fig. 3A). As previously reported [24], DU cells normally express K-RAS but, upon the 4-hydroxytamoxifen (4-OHT)-mediated stimulation of the Cre-ER^{T2} recombinase and the ensuing inactivation of the *Kras* gene, they lose the expression of the endogenous K-RAS protein and, therefore, become fully RAS-deficient (Supplementary Fig. 1A). K-RAS depletion caused a progressive reduction in the proliferation rates of these cells that eventually ended up with a total halt in cell division (Fig. 3B, C). It also promoted an abnormal enlargement in the size of the RAS-less MEFs (Fig. 3D, compare the top panels; see also Fig. 4C below). The terminal phenotype of these cells was maintained for 15 days (Fig. 3D, E) and even longer times (IF-P and XRB, unpublished data), as previously described

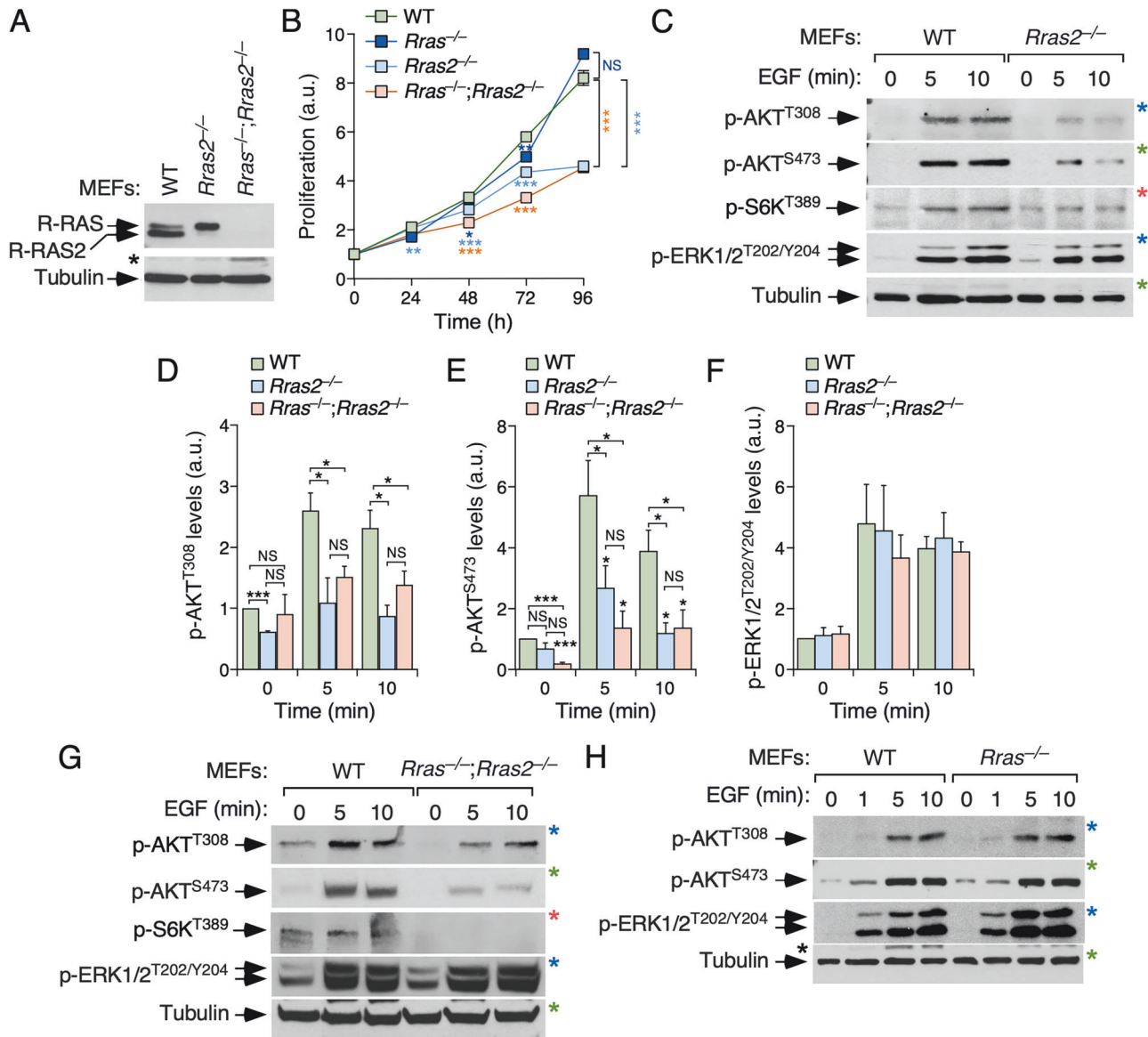


Fig. 1 Endogenous R-RAS2/TC21 is important for the signaling and proliferation of primary MEFs. **A** Expression levels of endogenous R-RAS2 and R-RAS proteins in primary MEFs of indicated genotypes (top panel). Levels of tubulin α were used as an internal loading control (bottom panel). WT, wild-type. **B** Proliferative activity of primary MEFs of indicated genotypes. a.u., arbitrary units. $*P \leq 0.05$; $**P \leq 0.01$; $***P \leq 0.001$ (two-way ANOVA test, $n = 4$ independent experiments). **C** Representative example of the phosphorylation levels of the indicated proteins and phosphosites (left) induced by EGF (10 ng/mL) in serum-starved MEFs of indicated genotypes. Levels of tubulin α were used as an internal loading control (bottom panel). p-, phosphorylated. The images of blots obtained from the same nitrocellulose filters are indicated by asterisks of the same color. **D–F** Quantification of the phosphorylation levels of indicated phosphosites of AKT (**D**, **E**) and ERK (**F**) in the experiments shown in (**C**, **G**). Data are represented as the fold-change variation as compared to the levels found in wild-type MEFs. The signals obtained with the tubulin α antibody were also used to normalize the values obtained among samples. $*P \leq 0.05$; $***P \leq 0.001$ relative to untreated DU derivatives cells (asterisks) or indicated paired controls (asterisk with brackets) (Student's *t*-test, $n = 5$ independent experiments for WT, $n = 3$ for *Rras2*^{-/-}, and $n = 3$ for *Rras*^{-/-}; *Rras2*^{-/-} MEFs). NS not statistically significant. **G**, **H** Representative example of the phosphorylation levels of the indicated proteins and phosphosites (left) induced by EGF (10 ng/mL) in serum-starved MEFs of indicated genotypes. Levels of tubulin α were used as an internal loading control (bottom panel). The images of blots obtained from the same nitrocellulose filters are indicated by asterisks of the same color. Data shown in **B**, **D–F** represent the means \pm SEM.

[24]. Furthermore, serum-starved RAS-less DU cells display statistically significant ERK phosphorylation defects after stimulation with platelet-derived growth factor (PDGF) (Supplementary Fig. 1B, top panel; quantitated in Supplementary Fig. 1C, left panel) or EGF (Supplementary Fig. 1D, top panels; quantified in Supplementary Fig. 1E, left panel). On the contrary, no statistically significant defect was detected in the phosphorylation of the S⁴⁷³ residue of AKT after stimulation of cells with PDGF (Supplementary Fig. 1B, middle panel; quantification in Supplementary Fig. 1C,

right panel) or EGF (Supplementary Fig. 1D, middle panels) (quantification in Supplementary Fig. 1E, right panel).

The shRNA-mediated depletion of endogenous R-RAS2/TC21 only induced minor proliferative defects at early timepoints (24–48 h) after deletion of the *Kras* gene in DU cells (Fig. 3B, C). This suggests that endogenous levels of R-RAS2 must be totally eliminated from MEFs (as in the case of knockout cells shown in Fig. 1) to significantly impact the proliferation of these cells. Alternatively, immortalization of DU cells can reduce their

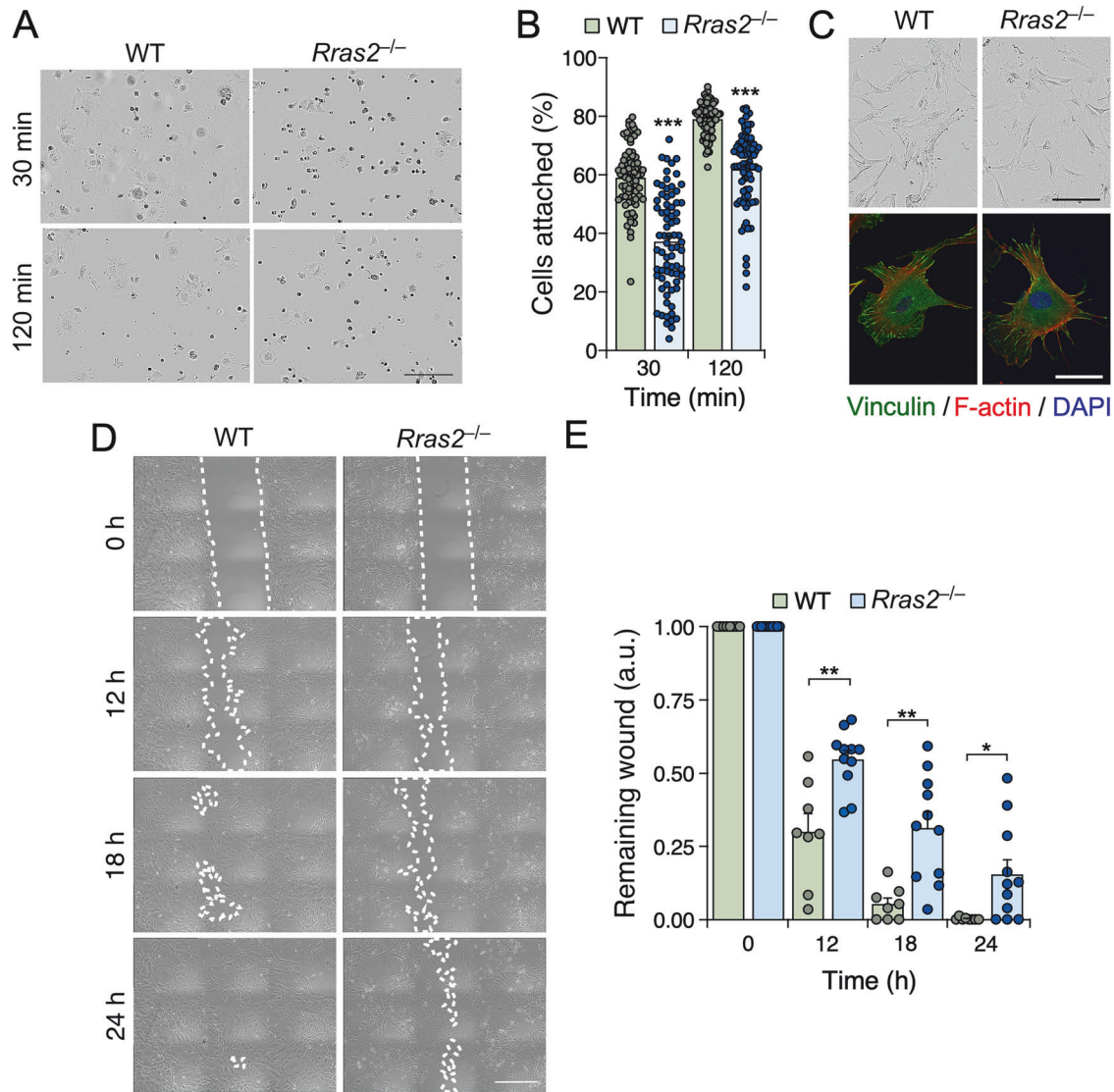


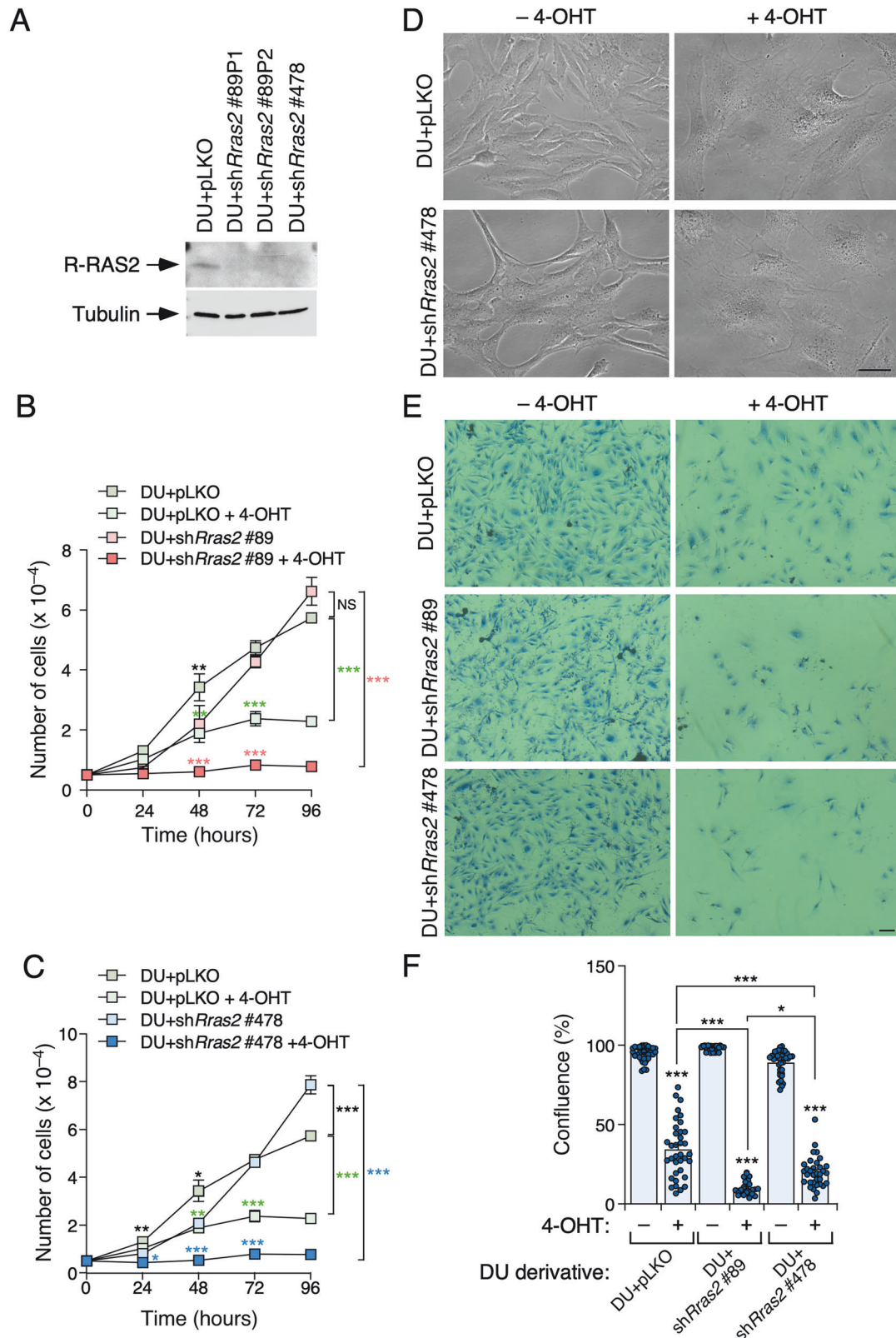
Fig. 2 Adhesion and wound healing properties of primary *Rras2*^{-/-} mouse embryonic fibroblasts. **A** Representative images of primary WT and *Rras2*^{-/-} MEFs at the indicated time points upon seeding. Images were taken at 10× magnification on the Incucyte[®] imaging system. Scale bar, 100 μ m. **B** Quantification of adherent cells at indicated times after plating. ***, $P \leq 0.001$, two-tailed Student's *t*-test ($n = 3$ independent experiments). **C** *Top panels*, representative images of indicated primary MEFs maintained onto fibronectin-coated plates. *Bottom panels*, representative images of indicated primary MEFs after staining with vinculin antibodies (green), rhodamine-phalloidin (red), and DAPI (blue) to show the localization of focal adhesions, F-actin, and nuclei, respectively. Scale bars, 200 μ m (upper panels) and 50 μ m (lower panels). **D** Representative images of primary wild-type and *Rras2*^{-/-} MEFs at indicated time points after removing the well insert and being recorded using the Nikon Eclipse TE2000-E microscope as indicated in Methods. Scale bar, 500 μ m. **E** Quantitation of the data obtained in (D) at indicated time points. Data are represented as the fold-change variation compared to levels found in time 0 of the experiment. * $P \leq 0.05$; ** $P \leq 0.01$, two-tailed Student's *t*-test ($n = 3$ independent experiments). In **B**, **E**, data represent the means \pm SEM.

dependency on R-RAS2 for proliferation unlike the case of primary MEFs (which are not immortalized). However, *Rras2* knockdown DU cells did exhibit cell adhesion defects (Supplementary Fig. 2A, quantification in Supplementary Fig. 2B) as previously seen in primary *Rras2*^{-/-} MEFs (Fig. 2A, B). This defect did not impair the proper adhesion of DU cells at later postplating time points (Supplementary Fig. 2C, compare first panel with rest of panels). These cells also display the typical enlargement in size of RAS-less MEFs (Fig. 3D, compare right panels). Notably, the depletion of the *Rras2* transcript exacerbated the proliferative defect that is induced under these RAS-less conditions (Fig. 3B, C). In addition, we observed a reduction in total cell number in RAS-less DU with depleted R-RAS2 at the final timepoint (15 days) of these experiments (Fig. 3E, F). This result indicates that the basal activity

of endogenous R-RAS2 is relevant for the long-term survival of MEFs lacking RAS proteins.

Constitutively active R-RAS2/TC21 rescues the lack of RAS GTPases in MEFs

Based on the above results, we investigated whether an active version of R-RAS2/TC21 could counteract the harmful effect of eliminating the three RAS proteins in MEFs. To this end, we ectopically expressed an active version of R-RAS2/TC21 (G23V mutant) in DU cells (Fig. 4A, B). Previous results have shown that this mutant version of R-RAS2 is highly transforming [7] and, given the structural similarity between R-RAS2 and RAS proteins, is likely that it will share biochemical (low intrinsic GTPase activity) and signaling (low RAF binding affinity) features similar to those



described for the analogous G12V mutant versions of RAS proteins [27]. Unlike the proliferation and morphology defects observed in 4-OHT-treated DU cells (see above, Fig. 3), RAS-less DU cells expressing R-RAS2^{G23V} maintained the normal morphology seen in wild-type DU cells (Fig. 4C, compare second and fourth columns

from left). In particular, they also exhibited higher proliferation rates than control DU cells not treated with 4-OHT (Fig. 4D). DU cells expressing R-RAS2^{G23V} also showed high levels of phosphorylation at both PKD1- (Fig. 4E, upper panel; compare lane 1 with lanes 7 and 10) and mTORC2-dependent (Fig. 4E, second panel

Fig. 3 R-RAS2/TC21 contributes to the proliferation and viability of RAS-less MEFs. **A** Expression levels of endogenous R-RAS2 (top panel) and tubulin α (bottom panel) in indicated DU cell derivatives (top). P1, pool 1; P2, pool 2. **B, C** Proliferative activity of the indicated DU cell derivatives that were untreated (-4-OHT) or treated ($+4\text{-OHT}$) with 4-hydroxytamoxifen as indicated (insets). $*P \leq 0.05$; $**P \leq 0.01$; $***P \leq 0.001$ (two-way ANOVA test, $n = 3$ independent experiments). **D** Representative images of the indicated DU cell derivatives (left) that were untreated (-4-OHT) or treated ($+4\text{-OHT}$) with 4-hydroxytamoxifen as shown (top). Scale bar, 50 μm . **E** Representative microscopy images of the indicated DU cell derivatives that were untreated ($-$) or treated ($+$) with 4-hydroxytamoxifen for 15 days and then stained with Giemsa. Scale bar, 50 μm . **F** Quantification of cell confluence obtained in the experiment shown in (**E**) using the Incucyte[®] AI Cell Health Analysis Software Module. $*P \leq 0.05$; $***P \leq 0.001$ relative to untreated DU cells (asterisks) or indicated paired controls (asterisks with brackets) (two-way ANOVA test, $n = 3$ independent experiments). Data shown in **B, C, F** represent the means \pm SEM.

from top; compare lane 1 with lanes 7 and 10) phosphosites of AKT under non-stimulation conditions regardless of the expression status of RAS proteins (quantification in Supplementary Fig. 3A, B). Consistent with this, the stimulation of these cells with PDGF resulted in minor changes (S^{473} site) or no changes (T^{308} site) in AKT phosphorylation levels relative to the values obtained in non-stimulated cells (Fig. 4E, first and second panels from top; quantification in Supplementary Fig. 3A and B). Similar results were observed in these cells when we monitored the phosphorylation levels of S6K (Fig. 4E, third panel from top).

Interestingly, we observed that R-RAS2^{G23V}-expressing DU cells displayed very low levels of ERK phosphorylation compared to controls after stimulation with PDGF (Fig. 4E, fourth panel from top, compare lanes 2–3 with lanes 8–9; quantification in Supplementary Fig. 3C). ERK phosphorylation levels were further reduced in RAS-deficient cells (Fig. 4E, fourth panel from top, compare lanes 7–9 with lanes 10–12; quantification in Supplementary Fig. 3C). These findings suggest that chronic stimulation of R-RAS2 activates a feedback mechanism that dampens ERK signaling in DU cells.

Constitutively active R-RAS does not rescue the lack of RAS GTPases in MEFs

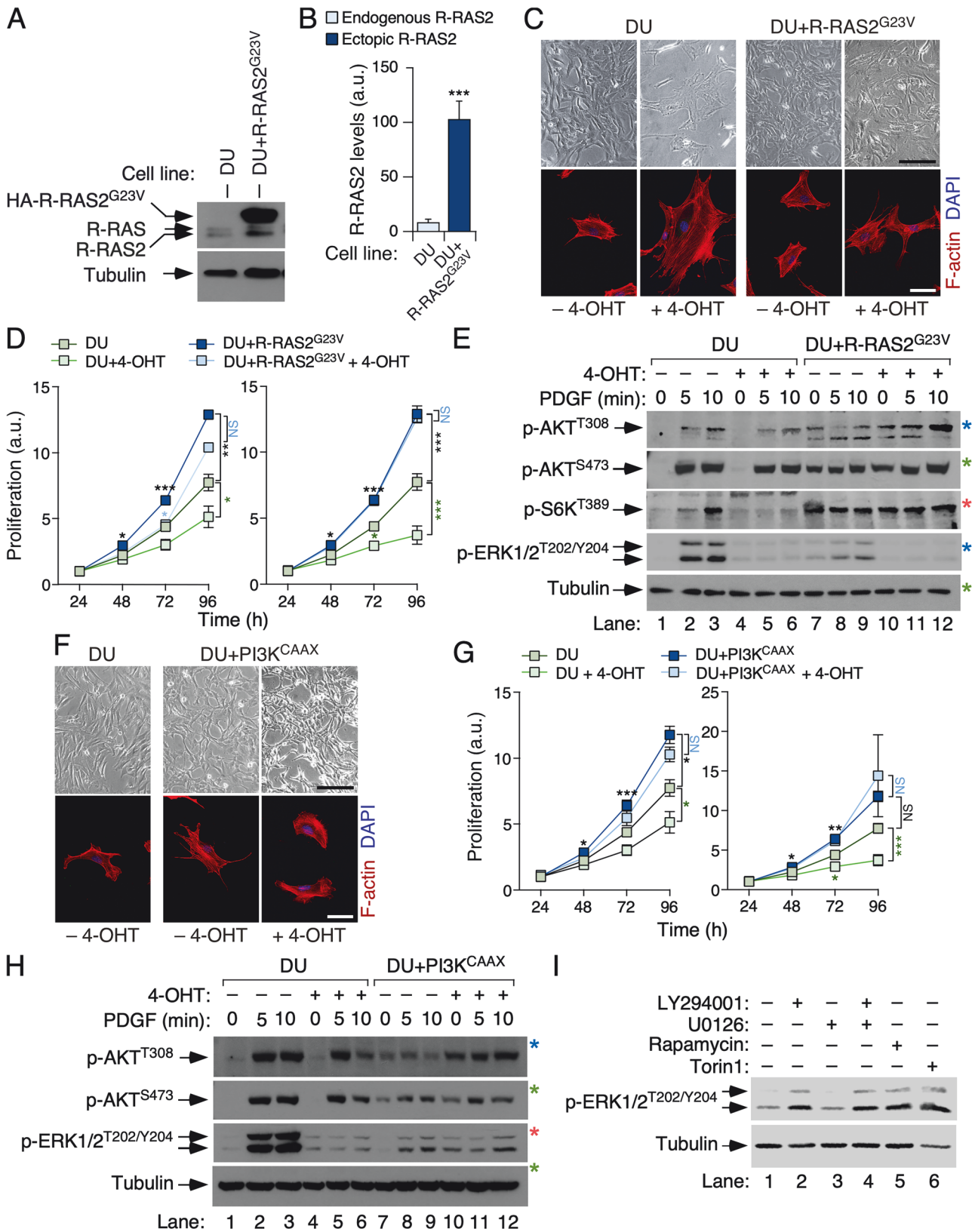
To verify that the rescue observed with R-RAS2^{G23V} was specific, we performed similar experiments using DU cells expressing R-RAS^{G38V} (for protein expression, see Supplementary Fig. 4A, top panel, lanes 7–12; see also Supplementary Fig. 4B for quantification of R-RAS abundance in these cells). G38V, like G23V in R-RAS2 and G12V in RAS proteins, is a gain-of-function mutation. Expression of R-RAS^{G38V} did not alter the normal AKT or ERK phosphorylation patterns of AKT or ERK in unstimulated and PDGF-stimulated DU cells (Supplementary Fig. 4A, see second, third, and fourth panels from top). Interestingly, these experiments indicated that the loss of RAS proteins triggers an increase in phospho-AKT levels in these cells in the absence of stimulation (Supplementary Fig. 4A, see second and third panels from top, compare lanes 7 and 10) that is not observed in control cells (Supplementary Fig. 4A, see second and third panels from top, lane 4; Supplementary Fig. 1). Unlike the case of R-RAS2^{G23V}, the ectopic expression of R-RAS^{G38V} did not rescue the morphological changes (Supplementary Fig. 4C) and the reduced cell proliferation rates (Supplementary Fig. 4D) typically observed in RAS-deficient DU cells. These results indicate that the rescue observed with R-RAS2^{G23V} is specific and not merely due to the over-expression of a RAS-related protein in RAS-deficient MEFs.

Constitutively active PI3K rescues the RAS-less phenotype in MEFs

Given the chronic stimulation of AKT observed in R-RAS2^{G23V}-expressing DU cells but not in the R-RAS^{G38V}-expressing counterparts, we next explored whether the rescue of the RAS-less phenotype by the former GTPase could be PI3K-mediated. To this end, we ectopically expressed in DU cells a mutant version of PI3K α containing the polybasic tail and the CAAX box of K-RAS4B at its C-terminus. This version of PI3K α , referred to hereafter as PI3K^{CAAX}, is constitutively active due to stable plasma membrane

tethering facilitated by the attached K-RAS4B C-terminal tail. Similar to R-RAS2^{G23V}-expressing cells, ectopic expression of PI3K^{CAAX} prevented the effects of the loss of the three RAS proteins on the morphology (Fig. 4F) and proliferation rates (Fig. 4G) of DU cells. It also promoted the constitutive phosphorylation of the PDK1- and mTORC2-dependent phosphosites of AKT both in the presence (Fig. 4H, two top panels, compare lane 1 with lanes 7 and 10) or absence of RAS protein expression (Fig. 4H, two top panels, compare lanes 1–3, 4–6 with lanes 10–12; quantification in Supplementary Fig. 3A, B). PI3K^{CAAX} also reduced ERK activation levels in PDGF-stimulated DU cells regardless of the recombination status of the *Kras* locus (Fig. 4H, third panel from top; quantification in Supplementary Fig. 3C). Interestingly, we found that basal phosphorylation levels of ERK found in DU cells expressing R-RAS2^{G23V} could be increased after treating the cells with inhibitors for PI3K α (LY294002) (Fig. 4I, compare lanes 1 and 2), mTORC1 (Rapamycin) (Fig. 4I, compare lanes 1 and 5), or mTORC1 plus mTORC2 (Torin1) (Fig. 4I, compare lanes 1 and 6). The addition of an inhibitor for MEK (U0126) did not have any effect on the basal levels of phospho-ERK found in R-RAS2^{G23V}-expressing DU cells (Fig. 4I, compare lanes 1 and 3). It did not abolish either the elevation of phospho-ERK levels induced by the LY294002 inhibitor (Fig. 4I, compare lanes 1, 2 and 4), indicating that the main input of the negative feedback between the PI3K and the ERK pathway must be located downstream of MEK in these cells. These results suggest that R-RAS2^{G23V} compensates for the loss of the three RAS proteins through chronic stimulation of the PI3K–AKT pathway. They also indicate that its rescue activity does not involve the restoration of normal levels of ERK signaling in RAS-deficient cells, which remain suppressed through a R-RAS2^{G23V}- and PI3K-regulated negative feedback mechanism that likely involves a downstream mTORC1 target.

To better understand the reduction in ERK phosphorylation seen in DU cells expressing R-RAS2^{G23V} or PI3K^{CAAX}, we performed immunoblot analyses to examine the effects of these two constitutively active proteins on components of the RAF–ERK pathway. We found that expression of R-RAS2^{G23V} or PI3K^{CAAX} in DU cells decreased phosphorylation of c-RAF (Supplementary Fig. 5A, top panels, compare lanes 2–3 with lanes 8–9 and lanes 14–15 with 20–21), MEK (Supplementary Fig. 5A, second panels from top, compare lanes 2–3 with lanes 8–9 and lanes 14–15 with 20–21), and RSK (Supplementary Fig. 5A, bottom panels, compare lanes 2–3 with lanes 8–9 and lanes 14–15 with 20–21) (quantification in Supplementary Fig. 5B–D). Interestingly, the negative impact of R-RAS2^{G23V} or PI3K^{CAAX} on the RAF–ERK axis progressively intensified from the most proximal (RAF) to the most distal (ERK, RSK) signaling elements of the pathway (Supplementary Fig. 5A–D). We also detected increased levels of phospho-c-RAF in nonstimulated DU cells expressing R-RAS2^{G23V} or PI3K^{CAAX} in the presence of K-RAS (Supplementary Fig. 5A, upper panels, compare lanes 1 with 7 and lane 13 with 19; quantification in Supplementary Fig. 5B). However, this phosphorylation was abolished upon K-RAS elimination in both cell variants (Supplementary Fig. 5A, upper panels, compare lanes 7–9 with lanes 10–12 and lanes 19–21 with lanes 22–24; quantification in Supplementary Fig. 5B). These findings suggest that the negative feedback mechanism



activated by R-RAS2^{G23V} or PI3K^{CAAX} predominantly affects MEK and ERK levels, with a lesser effect on c-RAF (Supplementary Fig. 5E). They also suggest that, in this cell system, the activation of c-RAF by R-RAS2^{G23V} or PI3K^{CAAX} is probably dependent on K-RAS (Supplementary Fig. 5E).

R-RAS2^{G23V} cannot overcome the lack of MEK or ERK in MEFs
The rescue obtained by R-RAS2^{G23V} or PI3K^{CAAX} under conditions of low levels of ERK signaling in RAS-less DU cells contradicted previous findings demonstrating the essentiality of ERK signaling for MEFs [26]. A possible explanation for this discrepancy is that

Fig. 4 R-RAS2^{G23V} rescues the lack of RAS GTPases in MEFs. **A** Representative immunoblot showing the expression levels of ectopic HA-tagged R-RAS2^{G23V} as well as of endogenous R-RAS and R-RAS2 (top panel) in lysates from indicated DU cell derivatives (top). Levels of tubulin α were used as an internal loading control (bottom panel). **B** Quantitation of endogenous wild-type R-RAS2 and ectopic R-RAS2^{G23V} proteins in the experiments shown in (A). *** $P \leq 0.001$ relative to control DU cells (Student's *t*-test, $n = 3$ experiments). **C** Representative images of indicated DU cell derivatives (top) treated (+4-OHT) or untreated (-4-OHT) with 4-hydroxytamoxifen. In the bottom panels, the cells were stained with rhodamine-phalloidin and DAPI to show the localization of F-actin and the nuclei, respectively. Scale bars, 40 μm (upper panels) and 25 μm (lower panels). **D** Proliferation of indicated DU derivatives treated (+4-OHT) or untreated (-4-OHT) with 4-hydroxytamoxifen (inset) using the MTT method. In the left panel, we show the proliferation of cells at early times (10 days) of the 4-OHT addition. In the right panel, we show the proliferation of cells at later times (20 days) after the 4-OHT administration. * $P \leq 0.05$; ** $P \leq 0.01$; *** $P \leq 0.001$ comparing DU with DU + 4-OHT (green asterisks), DU R-RAS2^{G23V} with DU R-RAS2^{G23V} + 4-OHT (blue asterisks), or DU with DU R-RAS2^{G23V} (black asterisks) (two-way ANOVA test, $n = 3$ independent experiments). **E** Phosphorylation levels of indicated proteins and phosphosites (left) in control cells (DU) and R-RAS2^{G23V}-expressing DU cells that were treated (+) or untreated (-) with 4-hydroxytamoxifen (top), serum starved and stimulated with PDGF (10 ng/mL) for the indicated times (top). Levels of tubulin α were used as an internal loading control (bottom panel). The images of blots obtained from the same nitrocellulose filters are indicated by asterisks of the same color. **F** Representative images of control DU cells and PI3K^{CAAX}-expressing DU cells that were either untreated (-4-OHT) or treated (+4-OHT) with 4-hydroxytamoxifen. In the bottom panels, the same cells were stained with rhodamine-phalloidin and DAPI to show the localization of F-actin and the nuclei, respectively. Scale bars, 40 μm (upper panels) and 25 μm (lower panels). **G** Proliferation of indicated DU derivatives treated (+4-OHT) or untreated (-4-OHT) with 4-hydroxytamoxifen (inset) measured as in (D). * $P \leq 0.05$; ** $P \leq 0.01$; *** $P \leq 0.001$ comparing DU with DU + 4-OHT (green asterisks), DU R-RAS2^{G23V} with DU R-RAS2^{G23V} + 4-OHT (blue asterisks), or DU with DU R-RAS2^{G23V} (black asterisks) (two-way ANOVA test, $n = 15$ for DU, $n = 5$ for DU + 4-OHT 1st period, $n = 5$ for DU + 4-OHT 2nd period, $n = 3$ for DU + PI3K^{CAAX}, and $n = 3$ for DU + PI3K^{CAAX} + 4-OHT). **H** Phosphorylation levels of proteins and phosphosites shown on the left in indicated serum starved DU cell derivatives treated (+) or untreated (-) with 4-OHT (top) that were stimulated with PDGF for indicated times as above (top). Levels of tubulin α were used as an internal loading control (bottom panel). The images of blots obtained from the same nitrocellulose filters are indicated by asterisks of the same color. **I** Top panel, phosphorylation levels of ERK in DU cells expressing R-RAS2^{G23V} that were treated with the indicated inhibitors (top). U0126 is an inhibitor for MEK. Bottom panel, levels of tubulin α in the same samples that were used as an internal loading control. Data shown in **B**, **D**, **G** represent the means \pm SEM.

RAS-deficient DU cells could retain a small pool of active ERK sufficient to maintain such proliferation rates when R-RAS2^{G23V} or PI3K^{CAAX} are present. In line with this possibility, we always found a residual level of phospho-ERK levels in RAS-less cells when analyzing long exposures of the immunoblots performed with anti-phospho-ERK antibodies (see above, Fig. 4E, fourth panel from top; Fig. 4H, third panel from top). To further address the issue of the requirement of ERK signaling for the rescue activity of the RAS-less phenotype by R-RAS2^{G23V}, we investigated whether this chronically activated mutant could rescue the MEK or ERK deficiency in MEFs. To this end, we ectopically expressed R-RAS2^{G23V} in the previously described *Map2k1*^{LoxP/LoxP}; *Map2k2*^{-/-} (designated hereafter as MEF^{ΔMEK} cells) and *Mapk1*^{LoxP/LoxP}; *Mapk3*^{-/-} (referred to hereafter as MEF^{ΔERK} cells) MEF cell lines [24, 26]. These cells, which already lack MEK2 (in the case of MEF^{ΔMEK}) or ERK1 (in the case of MEF^{ΔERK}), become totally deficient in MEK or ERK after the recombination of the *Map2k1* (encoding MEK1) or the *Mapk1* (encoding ERK2) loci induced upon the infection of cells with adenoviral particles encoding a Cre-GFP chimera [24, 26]. In MEF^{ΔMEK} cells, the constitutive expression of R-RAS2^{G23V} did not alter the general levels of ERK1 and ERK2 phosphorylation compared to controls (Fig. 5A, compare lanes 1 and 4). Similarly, R-RAS2^{G23V} did not affect basal ERK2 phosphorylation levels in MEF^{ΔERK} cells (Fig. 5B, compare lanes 1 and 3). In the latter case, only ERK2 is detected given that these cells have null *Mapk3* alleles [26]. In both cell models, however, the expression of R-RAS2^{G23V} increased the phosphorylation of AKT on the T³⁰⁸ site (Fig. 5A, B, third panels from top). After the Cre-mediated recombination step, the MEF^{ΔMEK} cells lost ERK phosphorylation due to complete loss of MEK proteins (Fig. 5A, lanes 2, 3 and 5). Similarly, MEF^{ΔERK} cells lost expression of ERK2 (Fig. 5B, lanes 2 and 4). Under these conditions, unlike the case of RAS-deficient DU cells (Fig. 4), the stable expression of R-RAS2^{G23V} could not rescue defects found in MEK-less MEFs (Fig. 5C–E) and ERK-deficient MEFs (Fig. 5F–H) despite inducing high levels of AKT phosphorylation (Fig. 5A, B, third panels from top). We also tried to use the inducible *Araf*^{LoxP/LoxP}; *Braf*^{LoxP/LoxP}; *Raf1*^{LoxP/LoxP} MEF model to assess the importance of RAF family members for the proliferation of R-RAS2^{G23V}-expressing cells [26]. However, the Cre-mediated recombination event in these cells consistently produced an active truncated version of RAF1 that prevented further evaluation of the rescue activity of

R-RAS2^{G23V} in cells deficient in RAF family kinases (IF-P and XRB, data not shown). These results suggest that R-RAS2^{G23V} likely requires some residual RAF–ERK signaling to rescue the RAS-deficient phenotype in MEFs.

To confirm these studies using an independent approach, we treated control DU cells and DU cells expressing R-RAS2^{G23V} with chemical inhibitors for PI3K α (LY294002); MEK (U0126); mTORC1 (Rapamycin); mTORC1 and mTORC2 (Torin1); or a combination of LY294002 plus U0126. Proliferation in controls and DU cells expressing R-RAS2^{G23V} was highly sensitive to Torin1, LY294002 + U0126 and, to a lesser extent, LY294002 alone while the effects of either U0126 or Rapamycin were less pronounced (Supplementary Fig. 6A and B). The proliferation of RAS-deficient DU cells expressing R-RAS2^{G23V} was also highly affected by Torin1 (Supplementary Fig. 6C). However, unlike the case of the other cell conditions tested in these analyses (Supplementary Fig. 6A, B), it was also highly sensitive to the single administration of either PI3K α or MEK inhibitors (Supplementary Fig. 6C). Consequently, the proliferation rates of those cells were not further decreased by the combined application of LY294002 plus U0126 (Supplementary Fig. 6C). The proliferation of RAS-less DU cells expressing R-RAS2^{G23V} was also inhibited by Rapamycin, although at lower levels than the rest of inhibitors tested (Supplementary Fig. 6C). Most inhibitors, except for U0126 in control cells (Supplementary Fig. 6D), also affected cell morphology and size in all DU cell variants used in these analyses (Supplementary Fig. 6D–F). The major effect was seen using the combination of LY294002 + U0126 inhibitors in control cells (Supplementary Fig. 6D) and R-RAS2^{G23V}-expressing cells (Supplementary Fig. 6E), although the synergism between these two drugs was lost in the case of the R-RAS2^{G23V}-expressing DU cells lacking RAS proteins (Supplementary Fig. 6F). Despite these effects, the treatments with these inhibitors could not elicit the morphological change that is typically observed in RAS-deficient DU cells (Supplementary Fig. 6G). This is consistent with our observations indicating that the generation of this morphological phenotype requires longer culture times than those used with chemical compounds. Taken together, these results further confirm that, at least in terms of cell proliferation, the rescue of the R-RAS2^{G23V}-mediated rescue of the RAS-deficient phenotype depends on high PI3K and mTORC activities as well as on the residual ERK signaling that is detected in RAS-less DU cells.

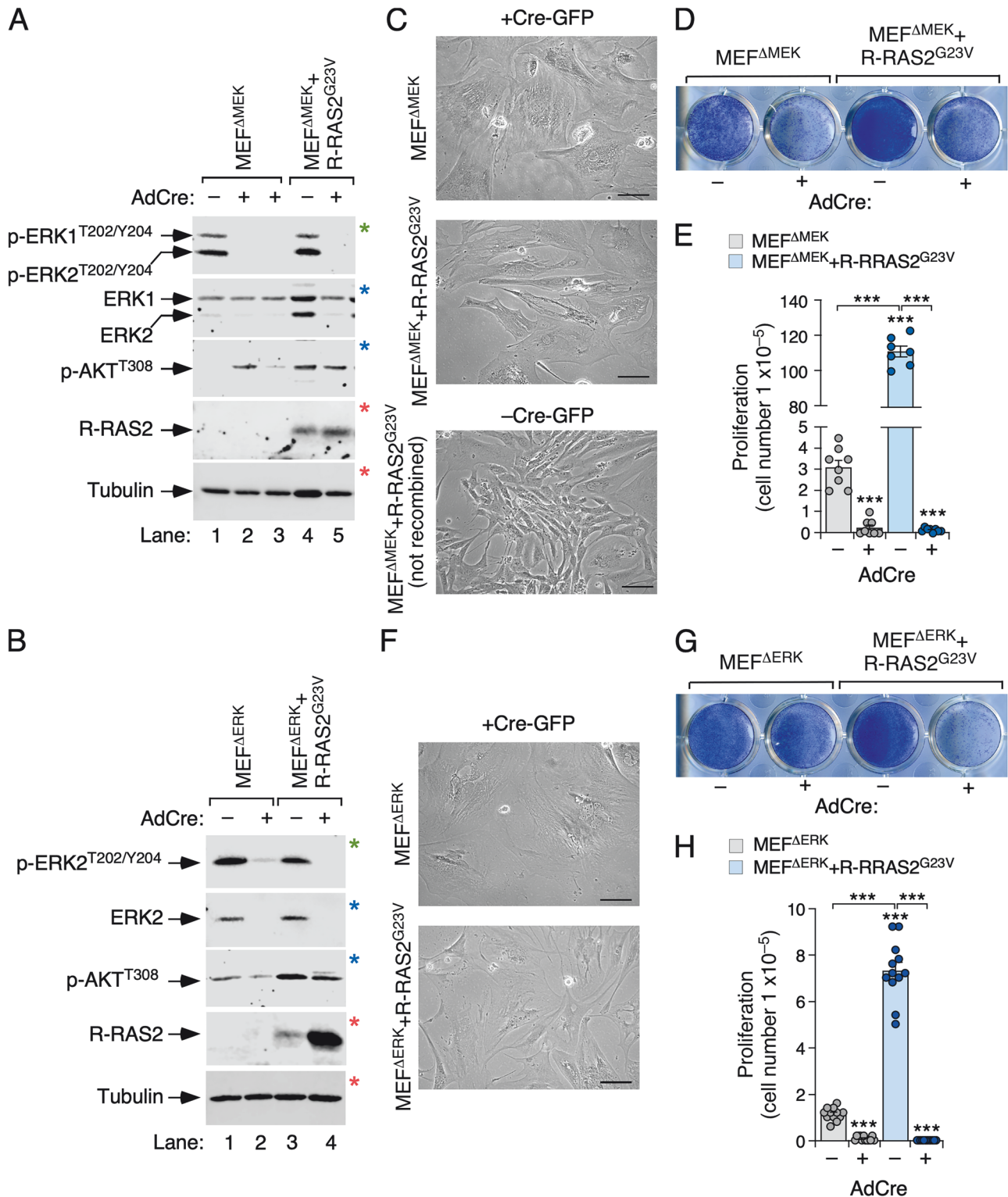


Fig. 5 R-RAS2^{G23V} cannot overcome the lack of MEK or ERK activity in MEFs. **A,B** ERK phosphorylation levels (top panels) and levels of indicated proteins (middle panels) in MEF^{ΔMEK} (**A**) and MEF^{ΔERK} (**B**) derivatives that were either not infected (-) or infected (+) with adenoviral particles encoding a Cre-GFP chimera (AdCre) as shown at the top. Levels of tubulin α were used as internal loading controls in both cases (**A** and **B**, bottom panels). The images of blots obtained from the same nitrocellulose filters are indicated by asterisks of the same color. Representative images of indicated AdCre-transduced MEF^{ΔMEK} cell derivatives (**C**) and MEF^{ΔERK} cell derivatives (**F**). In **C**, we also show a R-RAS2^{G23V}-expressing MEF^{ΔMEK} cell clone in which the recombination of the *Map2k1* locus did not take place (bottom panel). Scale bars, 50 μ m. **D, G** Representative scan images of Giemsa-stained MEF^{ΔMEK} cell derivatives (**D**) and MEF^{ΔERK} cell derivatives (**G**) that were either infected (+) or not infected (-) with adenoviral particles encoding AdCre as indicated (top). **E, H** Proliferation of MEF^{ΔMEK} cell derivatives (**E**) and MEF^{ΔERK} cell derivatives (**H**) seven days upon the AdCre infection (+) (bottom). *** $P \leq 0.001$ relative to untreated DU cells (asterisks) or indicated controls (asterisks with brackets) (Student's *t*-test, $n = 8$ in MEF^{ΔMEK} and $n = 12$ in MEF^{ΔERK}). Data shown in **E, H** represent the means \pm SEM.

R-RAS2^{G23V} and PI3K^{CAAX} promote overlapping transcriptional changes in DU cells

To further dissect the mechanism by which R-RAS2^{G23V} compensates functionally for the loss of RAS proteins, we conducted genome-wide expression profiling experiments in control DU cells and DU cells expressing either R-RAS2^{G23V} or PI3K^{CAAX} both before and after treatments with 4-OHT. Elimination of the three classical RAS proteins in control cells led to the downregulation of 538 genes (Supplementary Table 1) that were mostly linked to cell proliferation- and cytoskeletal-related biological processes according to standard functional annotation methods (Supplementary Fig. 7A, genes shown in blue). Furthermore, we found using gene set enrichment analyses (GSEA) downregulated gene signatures linked to MYC activity (Supplementary Fig. 7B) and mTORC1-related functions (Supplementary Fig. 7C). Conversely, the elimination of RAS proteins promoted the upregulation of a larger number of genes (871) that were mostly related to cytoskeletal-related processes (Supplementary Table 1 and Supplementary Fig. 7A, genes shown in red) and well-known TP53 transcriptional targets (Supplementary Fig. 7A, D, Supplementary Table 1) that were previously shown to be upregulated in RAS-less cells (*Cdkn2a*, *Cdkn2b*, *Gamt*, *Ndrp1*, *Perp*, *Sesn1*, *Spry2*, *Vdr*, *Ypel2*, *Ypel3*) [26]. This list does not include the *Trp53* mRNA (Supplementary Table 1), in agreement with previous results indicating that the activation of TP53 in RAS-less MEFs is mediated by a posttranslational, acetylation-mediated mechanism [26]. GSEAs also revealed that the upregulated gene subset contained enriched signatures for TP53 downstream transcription targets (Supplementary Fig. 7D) and cell senescence (Supplementary Fig. 7E).

In non-recombined DU cells, expression of R-RAS2^{G23V} or PI3K^{CAAX} led to the deregulation of 1110 common genes (654 upregulated, 456 downregulated) (Fig. 6A, B, Supplementary Table 2). In addition, we identified a subset of 1033 genes (414 upregulated, 619 downregulated) specifically deregulated in DU cells expressing PI3K^{CAAX} (Fig. 6A, B, Supplementary Table 2). Functional annotation analyses indicated that the genes commonly deregulated in cells expressing R-RAS2^{G23V} or PI3K^{CAAX} were primarily associated with the upregulation of cell proliferation and RNA-related processes (Fig. 6A, Supplementary Table 2). Interestingly, we also found the upregulation of several phosphatase-encoding transcripts (*Dusp5*, *Dusp6*, *Dusp7*, *Dusp14*) in this R-RAS2^{G23V}-PI3K^{CAAX} common transcriptome (Supplementary Table 2), which may contribute to the reduced ERK signaling previously seen in these cells (Fig. 4 and Supplementary Figs. S3 and S5). Unlike the case of normal DU cells (Supplementary Fig. 7), the treatment with 4-OHT only induced a minor effect (98 deregulated genes) in the transcriptome of R-RAS2^{G23V}-expressing DU cells (Fig. 6C, Supplementary Table 3). This indicates that: (i) the R-RAS2^{G23V}-regulated transcriptome of DU cells is fully RAS-independent; and (ii) that the ectopic expression of R-RAS2^{G23V} blocks the transcriptional changes triggered by the loss of RAS proteins in DU cells. In line with this, we did not detect in RAS-less cells expressing R-RAS2^{G23V} the upregulation of TP53 target genes and senescence-related signatures (Supplementary Table 3; IF-P and XRB, data not shown) [26] or the downregulation of MYC (Fig. 6D) and mTORC1 gene signatures (Fig. 6E) that were found in standard RAS-less DU cells. Collectively, these results indicate that chronic activation of the R-RAS2/TC21-PI3K axis overcomes the downregulation of MYC- and mTORC1-associated programs and the activation of TP53 that is associated with the loss of RAS function in DU cells.

Active R-RAS2/TC21 blocks TP53-dependent responses in RAS-less MEFs

To confirm our microarray data, we investigated whether the expression of R-RAS2^{G23V} blocked the induction of TP53-dependent responses previously described in RAS-less DU cells

[25, 26]. Using Western blot analyses, we found that the 4-OHT treatment increased the abundance in DU cells of typical TP53-regulated proteins such as p21^{CIP1} (Fig. 7A) and GADD45A (Fig. 7B). These changes take place even though the total amount of TP53 does not change under these conditions (Fig. 7C; quantification in Fig. 7D). Importantly, upregulation of p21^{CIP1} levels has been shown to be a critical event for the morphological and proliferative defects seen in RAS-less DU cells [26]. These experiments also revealed high basal levels of TP53 in DU cells expressing R-RAS2^{G23V} (Fig. 7C, D). However, this upregulation was diminished in 4-OHT-treated cells (Fig. 7C, D). These changes likely occur post-transcriptionally, as no variations were seen in the levels of *Trp53* mRNA between controls and DU cells expressing R-RAS2^{G23V} in our microarray experiments (Supplementary Tables 2 and 3).

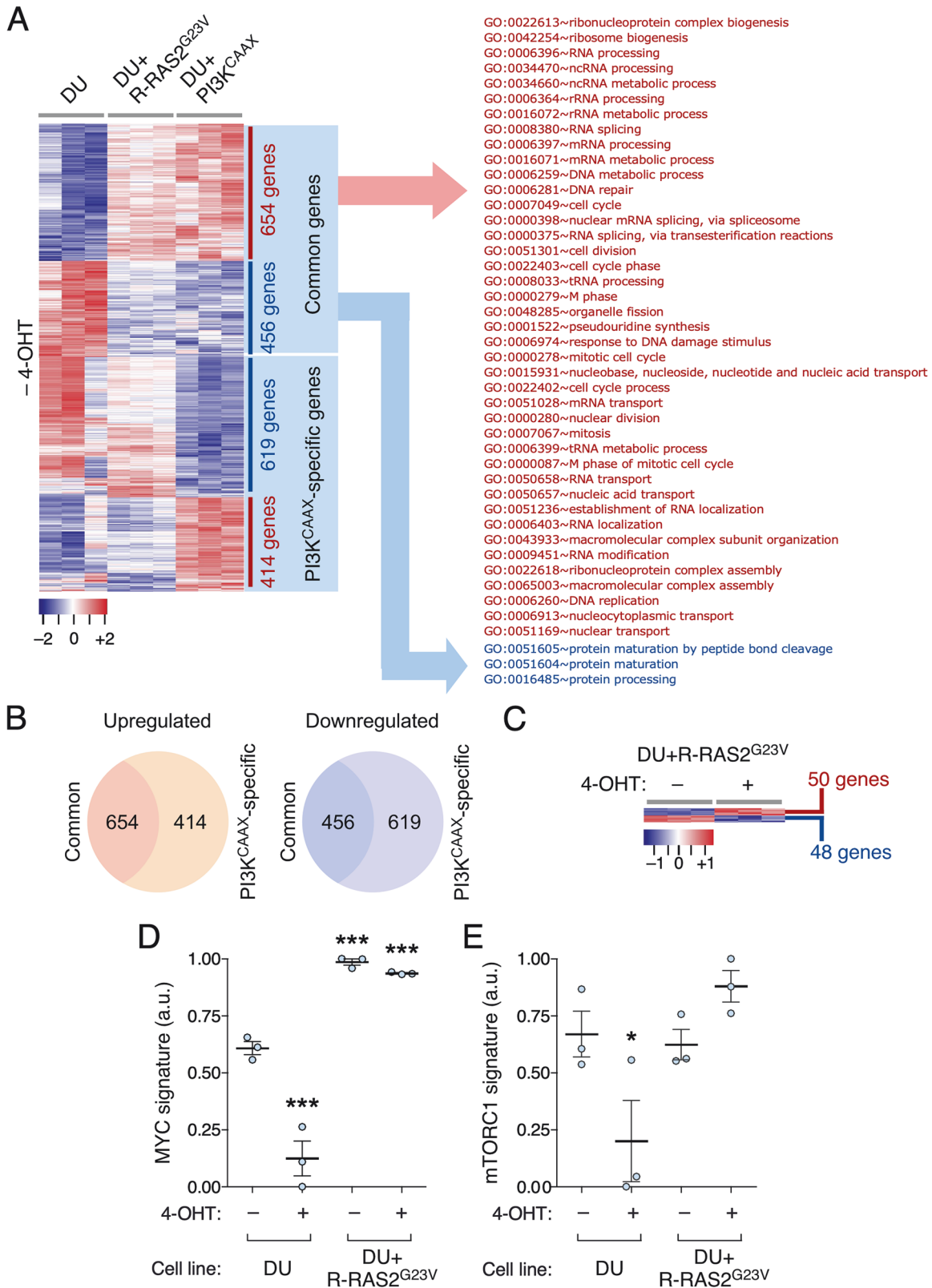
It is likely that TP53 is mostly inactive in DU cells expressing R-RAS2^{G23V}, as we could not detect statistically significant higher levels of p21^{CIP1} in these cells compared to controls (Fig. 7A, top panel; Fig. 7D). Likewise, we observed only minor changes in the abundance of GADD45A in those cells (Fig. 7B, upper panel; Fig. 7D, middle graph). Consistent with our microarray data (Supplementary Tables 2 and 3), we did not detect statistically significant changes in the levels of p21^{CIP1} or GADD45A in DU cells expressing R-RAS2^{G23V} after treatment with 4-OHT (Fig. 7A, B, D). Confirming the lack of proper activation of TP53 in these cells, we found using quantitative reverse transcription polymerase chain reactions (qRT-PCR) that TP53-regulated transcripts such as *Cdkn1a* (which encodes p21^{CIP1}), *Cdkn2a* (which encodes p14^{ARF}) and *Cdkn2b* (which encodes p15^{INK4B}) were not upregulated in DU cells expressing R-RAS2^{G23V} (Fig. 7E).

Given the above results, we also investigated whether R-RAS2^{G23V} could contribute to the inhibition of TP53 in other unrelated cell settings. To this end, we compared the response of control cells and R-RAS2^{G23V}-expressing DU cells to doxorubicin, a chemotherapy agent that triggers TP53-mediated apoptosis in cells [28, 29]. These experiments indicated that R-RAS2^{G23V}-expressing cells showed more resistance to this drug than control DU cells (Fig. 7F, G). This resistance was similar to that induced by the TP53 inhibitor pifithrin in doxorubicin-treated control cells (Fig. 7F, G). The inhibition of TP53 conferred by R-RAS2^{G23V} was only partial under these conditions, since the addition of pifithrin further increased the number of R-RAS2^{G23V}-expressing cells that remained viable upon exposure to the drug (Fig. 7F).

The lack of correlation between increased levels of TP53 and the amount of TP53 targets in R-RAS2^{G23V}-expressing DU cells led us to investigate the possible influence of the chronic activation of this GTPase on TP53 subcellular localization. To this end, we infected control cells and DU cells expressing R-RAS2^{G23V} or PI3K^{CAAX} with adenoviral particles encoding a GFP-tagged version of TP53 to monitor the subcellular localization of the fusion protein by confocal microscopy. These experiments showed that the GFP-TP53 protein predominantly localized in the nucleus of most control cells (Fig. 7H, I). In contrast, GFP-TP53 exhibited higher percentages in the cytosol or the cytosol plus nuclei in DU cells expressing R-RAS2^{G23V} or PI3K^{CAAX} (Fig. 7H, I). These results further suggest that TP53 is not properly activated in these two DU cell derivatives (Fig. 7J).

DISCUSSION

In this study, we explored the potential functional redundancy between the GTPase R-RAS2/TC21 and its closely related counterparts R-RAS and the three classical RAS proteins in MEFs. Although they belong to the same GTPase subfamily and share similar subcellular localization [2, 7–9], we found that the endogenous R-RAS2/TC21 and R-RAS proteins are not functionally redundant in this experimental model. More importantly, we found that endogenous R-RAS2/TC21 is important for the activation of the



PI3K–AKT axis as well as for the proliferation, cell adhesion, and wound-healing properties of primary MEFs. The role of R-RAS2/TC21 in proliferation of MEFs is particularly significant, given that the endogenous expression of oncogenic R-RAS2^{Q72L} at postnatal stages triggers an extensive mesenchymal hyperplasia that can eventually lead to fibrosarcoma formation in mice [3].

We also observed that endogenous R-RAS2/TC21 is important for the efficient adhesion and proliferation of immortalized DU cells during early postplating periods. This finding, along with previous observations in human cancer cell lines where the endogenous R-RAS2^{Q72L} mutant protein was knocked out [7], suggest that this GTPase plays a critical role in focal adhesion-

Fig. 6 R-RAS2^{G23V} and PI3K^{CAAX} promote overlapping transcriptional changes in DU cells. **A** Heatmap (left) and main functional annotation (right) of transcripts that are upregulated (red) or downregulated (blue) in R-RAS2^{G23V}-expressing DU cells or PI3K^{CAAX}-expressing DU cells versus the control DU cell line. Columns and rows represent independent replicas and single probe sets, respectively. The level of expression of probes is shown using a color gradient from dark blue (lowest expression) to dark red (highest expression) as indicated in the scale on the bottom. Total number of transcripts is indicated on the right of the heatmap. **B** Venn diagram representing the number of upregulated (left) or downregulated (right) genes that are common to R-RAS2^{G23V}-expressing cells and PI3K^{CAAX}-expressing cells or of those that are only detected in PI3K^{CAAX}-expressing DU cells. **C** Heatmap showing the transcripts that are upregulated (red) and downregulated (blue) upon the addition of 4-hydroxytamoxifen to R-RAS2^{G23V}-expressing DU cells. **C** Heatmap showing the transcripts that are upregulated (red) and downregulated (blue) upon the addition of 4-hydroxytamoxifen to R-RAS2^{G23V}-expressing DU cells. The level of gene expression is shown in a gradient from dark blue (lowest expression) to dark red (highest expression) as indicated in the scale on the bottom. Total number of transcripts is indicated on the right of the heatmap. **D, E** Dynamics of the MYC gene signature (**D**) and the mTORC1 gene signature (**E**) in indicated DU derivatives and RAS expression conditions (bottom). * $P \leq 0.05$; *** $P \leq 0.001$ relative to untreated control (ANOVA plus Dunnett test).

related processes. This can be related to the specific localization of endogenous R-RAS2/TC21 in these cytoskeletal structures [7]. Despite these functions, the basal activity of endogenous R-RAS2/TC21 is not sufficient to compensate for the loss of the three classical RAS proteins in DU cells (Supplementary Fig. 8, points a and b1). However, we did observe that the reduction in the levels of endogenous R-RAS2/TC21 accentuates the defects in proliferation, morphological shape, and long-term viability of DU cells lacking RAS proteins (Supplementary Fig. 8, point c). These results indicate that the signaling from R-RAS2/TC21 partially mitigates the adverse effects of the loss of classical RAS proteins in MEFs.

Based on the above results, we also decided to investigate whether a constitutively active version of R-RAS2/TC21 could counteract the activation of the TP53–p21^{CIP1}–retinoblastoma axis, which is responsible for the phenotype of RAS-less DU cells (for a scheme, see Supplementary Fig. 8, points a and b1) [26]. Our results indicated that the ectopic expression of R-RAS2^{G23V} or PI3K^{CAAX} does rescue the defects seen in these cells. We also found that this protective effect is mediated by the restoration of inhibition of TP53 in RAS-deficient cells, a process likely mediated by limiting the nuclear localization of this tumor suppressor protein (Supplementary Fig. 8, points d and e). The implication of R-RAS2^{G23V} in the inhibition of TP53 is probably more general, as we have observed that R-RAS2^{G23V}-expressing cells are also more resistant to potent apoptotic stimuli such as the chemotherapy compound doxorubicin. The resistance induced by R-RAS2^{G23V} in this setting, for example, is similar to that induced by a well-known TP53 inhibitor (pifithrin) in doxorubicin-treated control DU cells. However, unlike the case of the rescue of the RAS-less phenotype, the expression of R-RAS2^{G23V} only confers a partial resistance in this case to this TP53-mediated apoptotic response. This is likely due to the fact that the RAS-less phenotype is associated with a halt in cell proliferation that, probably, requires lower levels of TP53 activation than the apoptotic response that is rapidly triggered upon the addition of doxorubicin to cells. In addition to the inactivation of TP53, our present work also revealed that the chronic activation of the R-RAS2–PI3K pathway is associated with the activation of MYC-dependent and mTORC-dependent programs in these cells (Supplementary Fig. 8, points d and e).

Unlike other cell types in which active R-RAS2/TC21 proteins promote ERK stimulation [3, 7, 10, 11, 19], we have found in this work that R-RAS2^{G23V} seems to elicit a PI3K-dependent negative feedback mechanism that reduces the overall signaling of the ERK pathway in DU cells (Supplementary Fig. 8, point d). Consistent with this, we have found that the inhibition of PI3K and mTORC1 increases ERK phosphorylation in R-RAS2^{G23V}-expressing cells. Although we have not fully dissected this negative signaling crosstalk, our results using chemical inhibitors suggest that it is primarily established downstream of MEK. However, other crosstalk at the level of RAF and MEK family kinases are also probably in place (Supplementary Fig. 8, point d). We have also detected the upregulation of several *Dusp* family transcripts in DU cells expressing R-RAS2^{G23V} or PI3K^{CAAX} that could further contribute to the dampening of ERK signaling in those cells (Supplementary Fig. 8, point d).

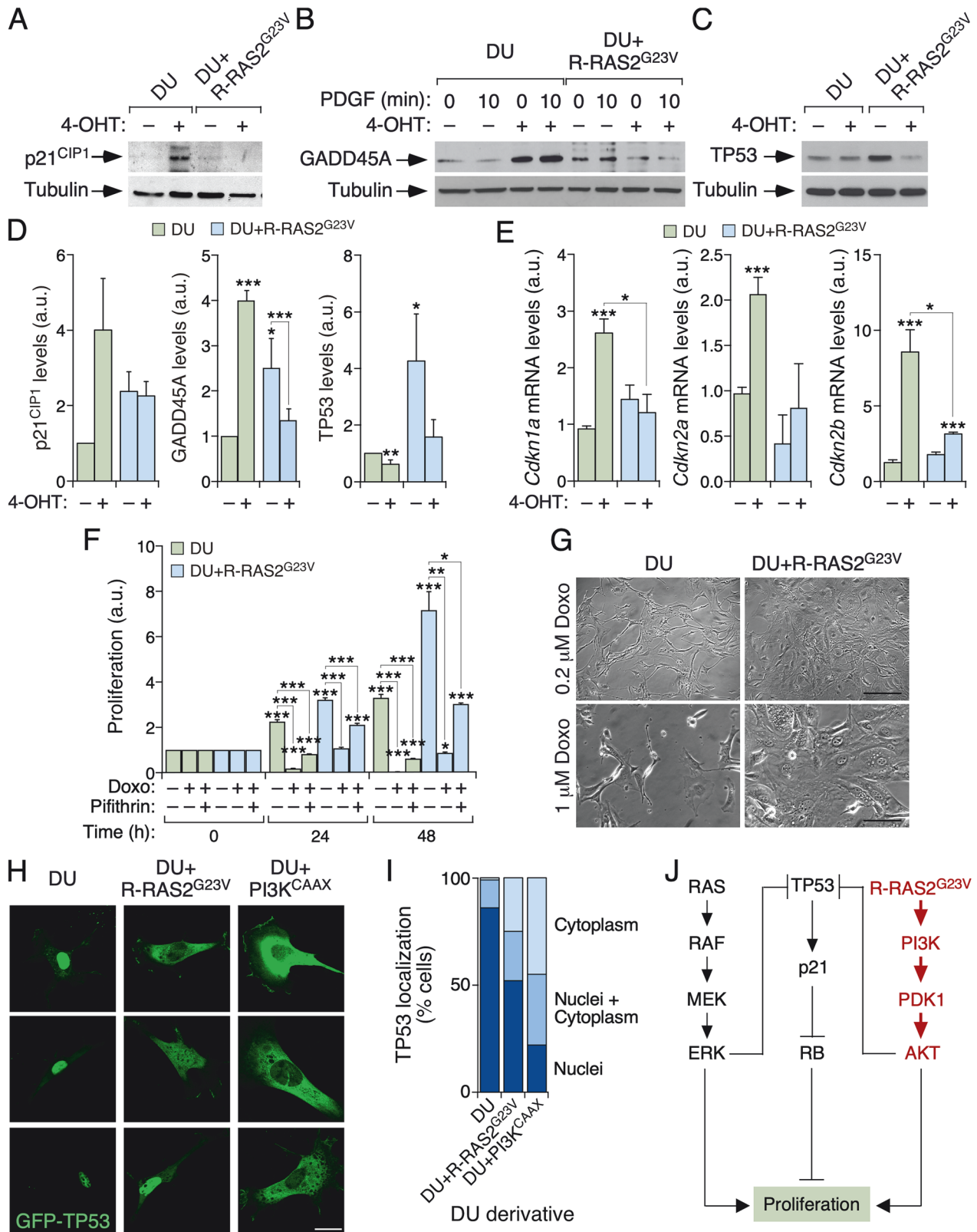
Despite these dampening effects on MEK and ERK signaling, our results indicate that a minimal output from MEK and ERK is still required to rescue the RAS-less phenotype by R-RAS2^{G23V}, as inferred from the observations made with MEK-less and ERK-less MEFs ectopically expressing R-RAS2^{G23V} (Supplementary Fig. 8, points f and g). Thus, we surmise that RAS-less DU cells keep a very small pool of active ERK through hitherto unknown compensatory mechanisms that is sufficient to ensure the rescue the proliferation and morphology in the presence of ectopically expressed R-RAS2^{G23V}. Another interesting observation from these signaling studies is that the elevation of c-RAF phosphorylation seen in DU cells expressing R-RAS2^{G23V} or PI3K^{CAAX} is totally abrogated upon elimination of K-RAS (Supplementary Fig. 5A, B). This result suggests that the simulation of c-RAF phosphorylation in these cells could be RAS-dependent. Whether this effect arises from direct or indirect stimulation of RAS guanosine nucleotide exchange factors in these conditions remains to be determined. Further studies will be needed to address all these issues.

We must note that a previous study conducted by some of us indicated that R-RAS2^{G23V} and two active versions of PI3K α (a myristoylated version and the gain-of-function H1047R mutant) were unable to rescue the proliferative defects of RAS-deficient DU cells [24]. The reason for the discrepancy between this earlier study and our current findings is unclear. A plausible possibility, however, is that this discrepancy arises from the different experimental models chosen in each study. Thus, in our case, we generated stable cell lines expressing R-RAS2^{G23V} or PI3K^{CAAX} and, subsequently, subjected them to the 4-OHT-mediated recombination step under subconfluent culture conditions. In contrast, the previous study used cells that were seeded at limited dilutions in the presence or absence of 4-OHT, and subsequently, the number of cell colonies formed was measured two weeks later [24]. It is likely that under these conditions the RAS-less cells could have been initially lost due to problems in cell adhesion or to the high levels of stress that are probably difficult to cope with at the earliest phases of the loss of K-RAS. Regardless of the reason involved, it is clear that MEFs lacking the three RAS proteins can be maintained with a wild-type-like phenotype for extended periods of time using our experimental model. This effect is specific given that the analogous R-RAS^{G38V} mutant cannot overcome the RAS-less phenotype when ectopically expressed in DU cells.

EXPERIMENTAL PROCEDURES

Ethics statement

All mouse experiments were performed according to protocols approved by the Bioethics Committee of the University of Salamanca and the animal experimentation authorities of the autonomous government of Castilla y León (Spain). The part of our study involving animal work is reported in accordance with the ARRIVE guidelines. No patients or patient-derived samples were used in this work. All experiments conducted in this study have been performed in accordance with relevant guidelines and regulations.



Mouse models

Rras2^{-/-} knockout and control mice have been described elsewhere [20, 30]. *Rras*^{-/-} mice were kindly provided by A.M. Chan (Department of Oncological Sciences, Mount Sinai School of Medicine, New York, NY, USA) [31]. *Rras*^{-/-}; *Rras2*^{-/-} mice were

generated by crossing the *Rras*^{-/-} and *Rras2*^{-/-} mouse strains. All animals were bred on the C57BL/6J genetic background. The animals were kept in a ventilated, pathogen-free facility at the University of Salamanca under controlled temperature (23 °C), humidity (50%), and a 12-hour-light/12-hour-dark cycle.

Fig. 7 R-RAS^{G23V} blocks TP53-dependent responses in RAS-less MEFs. **A–C** Representative immunoblot analyses showing the expression of indicated proteins in lysates (**A–C**, top panels) from the indicated DU cell derivatives and RAS-expression conditions. In **B**, the cells were also stimulated with PDGF (10 ng/mL) as indicated at the top. Levels of tubulin α were used as an internal loading control (**A–C**, bottom panels). **D** Quantification of the experiments shown in panel (**A**) (left), (**B**) (middle), and (**C**) (right). Values represent arbitrary densitometry units (with 1 assigned to the value obtained in control cells). * $P \leq 0.05$; *** $P \leq 0.001$ relative to untreated DU cells (asterisks) or indicated paired controls (asterisks with brackets) using two-tailed Student's t -test ($n = 3$ for p21^{CIP1}, 5 for GADD45A, and 3 for TP53). **E** Expression levels of the *Cdkn1a* mRNA (left), *Cdkn2a* mRNA (middle), and *Cdkn2b* mRNA (right) in indicated cells (top inset) and culture conditions (bottom). Values are given in arbitrary units, taking the lowest mean as 1. * $P \leq 0.05$; ** $P \leq 0.01$; *** $P \leq 0.001$ relative to either their own control or to the DU controls as indicated in the figure (two-tailed Student's t -test, $n = 4$ for *Cdkn1a*, 3 for *Cdkn2a*, and 3 for *Cdkn2b*). **F** Proliferation of indicated cells (inset) treated with 0.5 μ M doxorubicin and/or 1 μ M Pifithrin- α hydrobromide using the MTT method. * $P \leq 0.05$; ** $P \leq 0.01$; *** $P \leq 0.001$ relative to untreated DU cells (asterisks) or indicated paired samples (asterisks with brackets) (two-way ANOVA test, $n = 3$ technical replicates). **G** Representative images of indicated cells (top) that were treated with either 0.2 (top panels) or 1.0 μ M (bottom panels) doxorubicin. Scale bars, 40 μ m (upper panels) and 25 μ m (lower panels). Representative images (**H**) and quantitation (**I**) of the subcellular localization of ectopically expressed GFP-TP53 in indicated DU cell derivatives. $n = 105$ individual GFP-expressing DU cells, 75 individual GEF-expressing DU + R-RAS^{G23V} cells, and 81 individual GFP-positive DU + PI3K^{CAAX} cells. **J** Scheme with the results found in this figure. The connection of RAS proteins with TP53 has been described before [26, 28]. Data shown in **D–F** represent the means \pm SEM. Data shown in **I** represent the percentage of cells distributed in each analyzed parameter.

Plasmids

Lentiviral vectors encoding *Rras2*-targeting shRNAs (cat. no. TRCN0000311478, referred to as shRNA#478; and cat. no. TRCN0000354089, referred to as shRNA#89) or a scrambled shRNA control (TR1.5-pLKO-1-puro; cat. no. SHC001) were obtained from Sigma-Aldrich. Plasmids used in lentiviral particle generation, including pMD-G (cat. no. 187440) and psPax2 (cat. no. 12260) were obtained from Addgene. A pLVX-IRES-Hygro encoding the HA-tagged version of human R-RAS^{G23V} (pRL2) was obtained by directed mutagenesis of the previously described pRL1 vector [20] using the oligos hTC21G23V-3F (5'-GTG GTG GGC GGG GTC GGC GTG GGC AAG TCG-3') and hTC21G23V-3R (5'-CGA CTT GCC CAC GCC GAC CCC GCC GAC CAC CAC-3').

A lentiviral vector expressing the constitutively active version of bovine PI3K α (PI3K^{CAAX}) (pRL12) was generated by subcloning the cDNA present in the pSG5/5'MycTp110alpha^{CAAX} (kindly provided by J. Downward, The Crick Institute, London, UK) [32] into the BamHI-linearized pLVX-IRES-Hygro vector (cat. no. 632185, Clontech). To generate the lentiviral vector encoding an active version of R-RAS (G38V mutant) (pMFP44), the *Rras*^{G38V} cDNA was excised from the pCGN R-RAS38V (cat. no. #14728, Addgene) using BamHI, purified, and then ligated into the BamHI-linearized pLVX-IRES-ZsGreen1 vector (cat. no. 632187, Takara). Adenoviruses expressing murine GFP-TP53 (Adeno-Mmp53-GFP) were previously described by some of us [26].

Microbe strains

The *E. coli* DH5 α strain was used for cloning and plasmid generation.

Primary and immortalized MEF cells

Primary MEFs were isolated from 13.5-day-old WT, *Rras2*^{-/-}, *Rras*^{-/-} or *Rras*^{-/-}; *Rras2*^{-/-} embryos. The generation and characterization of the immortalized *Hras*^{-/-}; *Nras*^{-/-}; *Kras*^{Lox/Lox}; CreER^{T2} (DU), *Map2k1*^{LoxP/LoxP}; *Map2k2*^{-/-} (MEF ^{Δ MEK}), *Mapk1*^{LoxP/LoxP}; *Mapk3*^{-/-} (MEF ^{Δ ERK}), and *Araf*^{LoxP/LoxP}; *Braf*^{LoxP/LoxP}; *Raf1*^{LoxP/LoxP} MEF cell lines have been reported previously [24, 26]. All cells were grown in DMEM (Dulbecco's Modified Eagle Medium) supplemented with 10% fetal bovine serum, 1% L-glutamine, penicillin (10 μ g/mL) and streptomycin (100 μ g/mL) and maintained at 37 °C in a humidified 5% CO₂ atmosphere. Cells were dissociated using TrypLE™ Express (cat. no. 12604013, GIBCO). When indicated, cells were treated with LY294002 (10 mM, cat. no. S1105, Selleckchem), U0126 (25 mM, cat. no. S1102, Selleckchem), Rapamycin (10 nM, cat. no. S1039, Selleckchem), Torin 1 (250 nM, cat. no. S2827, Selleckchem) or a vehicle control (DMSO). After the cell treatment, plates were placed inside the Incucyte® system (Incucyte® SX5, Sartorius) to quantify cell number and surface area coverage as confluence

values every 24 h using the Incucyte® AI Cell Health Analysis Software Module. All Incucyte® experiments were performed in triplicate.

Western blotting

For analyses of total cell extracts, cells were washed in phosphate buffered saline solution twice and lysed in RIPA buffer (10 mM Tris-HCl [pH 7.5], 150 mM NaCl, 1% Triton X-100, 1 mM NaF, 1 mM Na₃VO₄, with a protease inhibitor tablet [cOmplete™, cat. no. 05056489001, Roche]). In the case of analyses of phosphorylated proteins, cells were washed as above and lysed in BLYS buffer (50 mM Tris-HCl [pH 7.5], 1 mM EGTA, 1 mM EDTA, 1% Triton X-100, 50 mM NaF, 1 mM Na₃VO₄, 5 mM Na₄P₂O₇, 0.27 M sucrose, 1 mM phenylmethylsulfonyl fluoride and a protease inhibitor tablet [cOmplete™]). In all cases, cellular extracts were precleared by centrifugation at 20,000 \times g for 10 min at 4 °C, denatured by boiling in 5x SDS-PAGE sample buffer, separated electrophoretically, and transferred onto nitrocellulose filters (cat. no. 2022-04-26, ThermoFisher Scientific) using the iBlot Dry Blotting System (cat. no. IB21001, ThermoFisher Scientific). Membranes were blocked in 5% bovine serum albumin (cat. no. A4503, Sigma-Aldrich) in TBS-T (25 mM Tris-HCl [pH 8.0], 150 mM NaCl, 0.1% Tween-20) for at least 1 h and then incubated overnight at 4 °C with the appropriate primary antibody. Primary antibodies used included those directed to R-RAS2 (an affinity-purified rabbit polyclonal antibody raised against the R-RAS2 C-terminal region [residues 183–198] that recognizes specifically R-RAS2 but not the related R-RAS or classical RAS proteins (ref no #1234, dilution 1:1000), R-RAS (C-19, cat. no. sc-523, Santa Cruz Biotechnology, dilution 1:1000), tubulin α (cat. no. CP06-100UG, Calbiochem, 1:2000 dilution), phospho-ERK1/2 (phospho-Thr²⁰² and phospho-Tyr²⁰⁴, cat. no. 4370, Cell Signaling Technology, 1:1000 dilution), phospho-AKT (p-Thr308, Cat. No. 4056, Cell Signaling Technology, 1:1000 dilution), phospho-AKT (phospho-Ser473, cat. no. 4051, Cell Signaling Technology, 1:1000 dilution), phospho-S6K (p-Thr389, Cat. No. 9205, Cell Signaling Technology, 1:1000 dilution), phospho-MEK1 (phospho-Ser²⁹⁸, cat. no. 98195, Cell Signaling Technology, 1:1000 dilution), p-RSK (phospho-Ser³⁸⁰, cat. no. 11989, Cell Signaling Technology, 1:1000 dilution), p-c-RAF (phospho-Ser³⁸⁸, cat. no. 9427, Cell Signaling Technology, 1:1000 dilution), and R-RAS (cat. no. sc-523, Santa Cruz Biotechnology, 1:1000 dilution). Membranes were then washed three times with TBS-T, incubated with the appropriate secondary antibody (ECL Rabbit IgG, HRP-linked whole Ab, cat. no. NA934-1ML, Amersham, 1:5000 dilution; ECL Mouse IgG, HRP-linked whole Ab, cat. no. NXA931-1ML, Amersham, 1:5000 dilution) for 60 min at room temperature and washed again three times as above. Immunoreactive bands were visualized using a chemiluminescent method

(ECL Pierce, cat. no. 32106, ThermoFisher Scientific). Bands were quantified using the ImageJ software, using the tubulin α signal as a normalization control among different samples.

Proliferation assays

For primary MEFs and DU cells, we assessed proliferation rates using the 3-(4,5-dimethylthiazol-2-yl) 2,5-diphenyltetrazolium bromide (MTT) method. Specifically, cells were seeded in 24-well plates at a density of 7×10^4 cells/well. At the indicated time points, the culture medium was replaced and 250 μ L of MTT solution (0.5 mg/mL) were added. After incubation for 1 h at 37 °C in a 5% CO₂ atmosphere, the MTT solution was replaced with 500 μ L of dimethyl sulfoxide to dissolve the formazan crystals that had formed and, 15 min later, the absorbance at 570 nm was measured in a Tecan Ultra Evolution plate reader. For MEF ^{Δ ERK} and MEF ^{Δ MEK} cells, the Cre-recombined cells were seeded at a concentration of 7×10^4 cells/mL onto 24-well plates. At the indicated time points, cells were harvested, diluted in Beckman Counter ISOTON II (cat. no. 8448011, Beckman), and counted using the Beckman Coulter Z1 apparatus. For the R-RAS^{G38V}-expressing DU cell line, cells were seeded at a density of 7×10^4 cells/well as above and cell proliferation quantified by counting the number of phase objects over time using the Incucyte[®] AI Cell Health Analysis Software Module.

Cell adhesion

For primary *Rras2*^{-/-} MEFs and controls, we plated 4×10^4 cells on fibronectin-coated P24 plates and assessed cell adhesion at specified intervals using the Incucyte[®] AI Cell Health Analysis Software Module. This software was configured to distinguish cells in suspension and cells attached to the plate. For DU cell lines, 4×10^4 cells were seeded as above and photographed 30 minutes later to quantify the number of attached cells.

Immunofluorescence and F-actin staining

DU cells, RRAS2^{G23V}-expressing cells, PI3K^{CAAX}-expressing cells, or sh*Rras2* (#89 and #478)-expressing DU cells were cultured onto coverslips treated with 2 μ g/mL fibronectin in imaging buffer (20 mM HEPES [pH 7.4], 140 mM NaCl, 2.5 mM KCl, 1.8 mM CaCl₂ and 1 mM MgCl₂) for 1 h at 37 °C. Cells were then fixed in 4% formaldehyde in phosphate-buffered saline for 10 min at room temperature. After two washes with phosphate-buffered saline, cells were permeabilized with 0.3% Triton X-100 (cat. no. X100, Sigma-Aldrich) in phosphate-buffered saline for 10 min at room temperature, followed by three washes with phosphate-buffered saline. Cells were then blocked in 2% bovine serum albumin (cat. no. MB04603, NZYtech) in TBS-T for 30–45 min in a wet chamber. Where indicated, cells were incubated for 2 h at room temperature with antibodies to vinculin (cat. no. V9131, Sigma-Aldrich, diluted 1:5000 in blocking buffer), washed three times in TBS-T, and then incubated with goat anti-mouse IgG antibodies coupled to Alexa Fluor 488 (cat. no. A32723, Invitrogen, 1:400 dilution) for 30 min at room temperature. Cells were subsequently stained with rhodamine phalloidin (cat. no. R415, Thermo Fisher Scientific, dilution 1:400) for 30 min at room temperature. After two additional washes with TBS-T, cells were stained with 1 μ g/mL of 4',6-diamidino-2-phenylindole (cat. no. D1306, Invitrogen) for 3 min to visualize the nuclei. Coverslips were mounted on microscopy slides with Mowiol medium (cat. no. 475904, Merck) for analysis using a Laser Scan Leica SP8 Confocal Microscopy.

Wound healing assays

We plated 7×10^3 MEFs of indicated genotypes per Culture-Insert 3 well (cat.no. 80366, Ibidi) in a volume of 70 μ L/well. After cell attachment, the insert present in the well was removed to create a gap in the cell monolayer. The filling of this gap by cells was monitored in real-time using the Nikon Eclipse TE2000-E until the wound closure was observed. The percentage of wound closure at specified experimental time points was determined using images

from the recorded movies, which were analyzed utilizing the ImageJ2 software (version 2.14).

Generation of knockout MEF cells

To eliminate endogenous *Kras*, DU cells were treated with 0.6 mM of 4-OHT (cat. no. S8956, Selleckchem) for 15 days. For generating ERK-less or MEK-less cells, the appropriate MEF cell lines (see above) were transduced with adenoviral particles encoding a Cre-GFP fusion (Ad5CMVCre-eGFP, cat. no. VVC-U of Iowa-1174, UI Viral Vector Core Web, Carver College of Medicine, University of Iowa, Iowa City, IA, USA) in 500 μ L with a multiplicity of infection of 100 for 30 min, followed by the addition of 9.5 mL of complete medium were added to 10 cm Petri dishes.

Production of viral particles

To generate viral particles, HEK293T cells (cat. no. CRL-1573, American Type Culture Collection) were cultured as described above and transfected with appropriate lentiviral plasmids (10 μ g) along with 5 μ g of pMD-G and 7.5 μ g of pPax2 using the JetPEI transfection reagent (cat. no. 101-10 N, Polyplus). Lentivirus-containing supernatants were collected, passed through 0.45 μ m filters (cat. no. 10462100, GE Healthcare), and used to infect the parental cells in a 1:1 ratio.

shRNA-mediated depletion of endogenous R-RAS2/TC21

DU cells were infected in the presence of 8 μ g/mL polybrene (cat. no. H9268-5G, Sigma-Aldrich) with the indicated shRNA-encoding lentiviruses. Forty-eight hours post-transduction, cells were subjected to puromycin selection (2 μ g/mL, cat. no. P8833, Sigma-Aldrich). Proper depletion of endogenous R-RAS2/TC21 was confirmed by immunoblotting.

Generation of MEF derivatives

To generate R-RAS2^{G23V}-expressing DU cells, MEF ^{Δ MEK} cells, MEF ^{Δ ERK} cells, and MEF ^{Δ RAF} cells, we infected the appropriate cell line with lentiviruses produced from the pRL2 plasmid in the presence of 8 μ g/mL polybrene. PI3K^{CAAX}-expressing DU cells and R-RAS^{G38V}-expressing DU cells were created similarly by infecting cells with lentiviruses generated from the pRL12 and pMFP44 plasmids, respectively. Cells transduced with R-RAS2^{G23V}-encoding lentiviruses were selected with hygromycin (800 μ g/mL) 48 h post-transduction. In the case of cells transduced with R-RAS^{G38V}-encoding lentiviral particles, they were selected based on GFP positivity by flow cytometry. After selection, 0.6 μ M 4-OHT was applied to the cultures to generate RAS-less cells, MEK-less cells, ERK-less cells, or RAF-less cells as indicated above.

Cell staining with Giemsa

Cells were fixed with 10% formaldehyde for 10 min and stained for 10 min with a Giemsa solution (cat. no. G580, Sigma-Aldrich) diluted 1:7 in distilled deionized water. After staining, the solution was then removed, and the plates were washed five times with distilled, deionized water before and air-drying at room temperature. Stained cells were imaged using a Nikon Eclipse Ti-S microscope and an EPSON V700 scanner. To quantify cell confluence, images were captured with the Incucyte[®] reader and analyzed using the AI Cell Health Analysis Software Module.

Gene expression profiling

Total RNAs from DU, DU + R-RAS2^{G23V} and DU- + PI3K^{CAAX} cells were isolated using the RNAeasy Mini Kit (cat. no. 74104, Qiagen) and analyzed using Affymetrix microarrays (Clariom[™] S Assay HT) at the CIC Genomics Core Facility according to manufacturer's recommendations.

Bioinformatics of microarray data

Statistical analyses were done using R (version 3.6.3), along with Python (version 3.9.0) for text file processing. Signal intensity

values were obtained from expression microarray CEL files using robust multichip average. Differentially expressed genes were identified using linear models for microarray data (limma) [33]. Adjusted *P* values for multiple comparisons were calculated using the Benjamini-Hochberg correction (FDR). Gene Ontology and KEGG pathway enrichment analyses were performed using DAVID (<https://david.ncicrf.gov>) [34, 35]. Expression heatmaps were generated using the heatmap3 R package (<http://CRAN.R-project.org/package=corrplot>). Gene set enrichment analyses (GSEA) [36] were performed with defined gene sets using gene set permutations ($n = 1000$) for significance assessment and signal-to-noise metrics for ranking genes. The gene sets used were from the Molecular Signatures (MSigDB v7.2). Enrichment scores were calculated using single-sample GSEA [36, 37].

Determination of mRNA abundance

Total RNA was extracted using either the NZYol (cat no. MB18501, NZYTech) or the RNeasy Mini Kit (cat. no. 74104, Qiagen) and analyzed by qRT-PCR using the Power SYBR Green RNA-to-CT 1-Step Kit (cat. no. 4389986, Applied Biosystems) and the StepOnePlus Real-Time PCR System (cat. no. 4376600, Applied Biosystems). Raw qRT-PCR data were analyzed using the StepOne software v2.1 (Applied Biosystems), using the abundance of the endogenous *Gapdh* mRNA as the internal normalization control. Primers used for transcript quantitation included 5'-GCA TGG ACG ATC TGT TGC TG-3' (forward) and 5'-CTG TCC CAG ACT GCA GGA AG-3' (reverse) for *Tp53* cDNA; 5'-ACG TGG CCT TGT CGT TGT CT-3' (forward) and 5'-GAC CAA TCT GCG CTT GGA GTG-3' (reverse) for *Cdkn1a* cDNA; 5'-GAG CCG GCG GAG ACA TTG GG-3' (forward) and 5'-TGG CCA CCT CCA CCA AGC CT-3' (reverse) for *Gadd45b* cDNA; and 5'-TGG ACC AAC TGC TTA GC-3' (forward) and 5'-TCT TCT GGG TGG CAG TGA TG-3' (reverse) for *Gapdh* cDNA.

Statistics

Statistical analyses were performed using GraphPad Prism software (version 9.0). The number of biological replicates (n), statistical tests performed, and statistical significance levels are indicated for each experiment in the figure legends as well as in the results section of this document. Data were analyzed using Student's *t*-test, two-way ANOVA, or ANOVA with Dunnett tests as noted in the figure legends. In all cases, values were considered significant when $P \leq 0.05$. Unless otherwise stated, data are presented as the mean \pm SEM.

DATA AVAILABILITY

Microarray data reported in this paper have been deposited in the GEO database (<https://www.ncbi.nlm.nih.gov/geo/>) under the accession number GSE256253.

MATERIALS AVAILABILITY

All relevant data are available from the corresponding author upon reasonable request. A Materials Transfer Agreement could be required in the case of potential commercial applications.

REFERENCES

- Drivas GT, Shih A, Coutavas E, Rush MG, D'Eustachio P. Characterization of four novel ras-like genes expressed in a human teratocarcinoma cell line. *Mol Cell Biol*. 1990;10:1793–8.
- Weber SM, Carroll SL. The role of R-Ras proteins in normal and pathologic migration and morphologic change. *Am J Pathol*. 2021;191:1499–510.
- Fernández-Pisonero I, Clavaín L, Robles-Valero J, Lorenzo-Martín LF, Caloto R, Nieto B, et al. A hotspot mutation targeting the R-RAS2 GTPase acts as a potent oncogenic driver in a wide spectrum of tumors. *Cell Rep*. 2022;38:110522.
- Niihori T, Nagai K, Fujita A, Ohashi H, Okamoto N, Okada S, et al. Germline-activating RAS2 mutations cause Noonan syndrome. *Am J Hum Genet*. 2019;104:1233–40.
- Hortal AM, Oeste CL, Cifuentes C, Alcoceba M, Fernández-Pisonero I, Clavaín L, et al. Overexpression of wild type RAS2, without oncogenic mutations, drives chronic lymphocytic leukemia. *Mol Cancer*. 2022;21:35.
- Cifuentes C, Oeste CL, Fernández-Pisonero I, Hortal AM, García-Macias C, Hochart J, et al. Unmutated RAS2 emerges as a key oncogene in post-partum-associated triple negative breast cancer. *Mol Cancer*. 2024;23:142.
- Clavaín L, Fernández-Pisonero I, Movilla N, Lorenzo-Martín LF, Nieto B, Abad A, et al. Characterization of mutant versions of the R-RAS2/TC21 GTPase found in tumors. *Oncogene*. 2023;42:389–405.
- Furuhjelm J, Peränen J. The C-terminal end of R-Ras contains a focal adhesion targeting signal. *J Cell Sci*. 2003;116:3729–38.
- Ohba Y, Mochizuki N, Yamashita S, Chan AM, Schrader JW, Hattori S, et al. Regulatory proteins of R-Ras, TC21/R-Ras2, and M-Ras/R-Ras3. *J Biol Chem*. 2000;275:20020–6.
- Graham SM, Cox AD, Drivas G, Rush MG, D'Eustachio P, Der CJ. Aberrant function of the Ras-related protein TC21/R-Ras2 triggers malignant transformation. *Mol Cell Biol*. 1994;14:4108–15.
- Movilla N, Crespo P, Bustelo XR. Signal transduction elements of TC21, an oncogenic member of the R-Ras subfamily of GTP-binding proteins. *Oncogene*. 1999;18:5860–9.
- Graham SM, Oldham SM, Martin CB, Drugan JK, Zohn IE, Campbell S, et al. TC21 and Ras share indistinguishable transforming and differentiating activities. *Oncogene*. 1999;18:2107–16.
- Lowe DG, Goeddel DV. Heterologous expression and characterization of the human R-ras gene product. *Mol Cell Biol*. 1987;7:2845–56.
- Saez R, Chan AM, Miki T, Aaronson SA. Oncogenic activation of human R-ras by point mutations analogous to those of prototype H-ras oncogenes. *Oncogene*. 1994;9:2977–82.
- Cox AD, Brtva TR, Lowe DG, Der CJ. R-Ras induces malignant, but not morphologic, transformation of NIH3T3 cells. *Oncogene*. 1994;9:3281–8.
- Calvo F, Crespo P. Structural and spatial determinants regulating TC21 activation by RasGRF family nucleotide exchange factors. *Mol Biol Cell*. 2009;20:4289–302.
- Zhang X, Spiegelman NA, Nelson OD, Jing H, Lin H. SIRT6 regulates Ras-related protein R-Ras2 by lysine defatty-acylation. *Elife*. 2017;6:4302.
- López-Barahona M, Bustelo XR, Barbacid M. The TC21 oncoprotein interacts with the Ral guanosine nucleotide dissociation factor. *Oncogene*. 1996;12:463–70.
- Rosario M, Paterson HF, Marshall CJ. Activation of the Raf/MAP kinase cascade by the Ras-related protein TC21 is required for the TC21-mediated transformation of NIH 3T3 cells. *EMBO J*. 1999;18:1270–9.
- Larive RM, Abad A, Cardaba CM, Hernandez T, Canamero M, de Alava E, et al. The Ras-like protein R-Ras2/TC21 is important for proper mammary gland development. *Mol Biol Cell*. 2012;23:2373–87.
- Graham SM, Vojtek AB, Huff SY, Cox AD, Clark GJ, Cooper JA, et al. TC21 causes transformation by Raf-independent signaling pathways. *Mol Cell Biol*. 1996;16:6132–40.
- Patmore DM, Welch S, Fulkerson PC, Wu J, Choi K, Eaves D, et al. In vivo regulation of TGF-beta by R-Ras2 revealed through loss of the RasGAP protein NF1. *Cancer Res*. 2012;72:5317–27.
- Huang Y, Rangwala F, Fulkerson PC, Ling B, Reed E, Cox AD, et al. Role of TC21/R-Ras2 in enhanced migration of neurofibromin-deficient Schwann cells. *Oncogene*. 2004;23:368–78.
- Drosten M, Dhawahir A, Sum EY, Urošević J, Lechuga CG, Esteban LM, et al. Genetic analysis of Ras signalling pathways in cell proliferation, migration and survival. *EMBO J*. 2010;29:1091–104.
- Drosten M, Barbacid M. Ras and p53: an unsuspected liaison. *Mol Cell Oncol*. 2016;3:e996001.
- Drosten M, Sum EY, Lechuga CG, Simón-Carrasco L, Jacob HK, García-Medina R, et al. Loss of p53 induces cell proliferation via Ras-independent activation of the Raf/Mek/Erk signaling pathway. *Proc Natl Acad Sci USA*. 2014;111:15155–60.
- Hunter JC, Manandhar A, Carrasco MA, Gurbani D, Gondi S, Westover KD. Biochemical and structural analysis of common cancer-associated KRAS mutations. *Mol Cancer Res*. 2015;13:1325–35.
- Lowe SW, Ruley HE, Jacks T, Housman DE. p53-dependent apoptosis modulates the cytotoxicity of anticancer agents. *Cell*. 1993;74:957–67.
- Lowe SW, Bodis S, McClatchey A, Remington L, Ruley HE, Fisher DE, et al. p53 status and the efficacy of cancer therapy in vivo. *Science*. 1994;266:807–10.
- Delgado P, Cubelos B, Calleja E, Martínez-Martín N, Cipres A, Merida I, et al. Essential function for the GTPase TC21 in homeostatic antigen receptor signaling. *Nat Immunol*. 2009;10:880–8.
- Singh G, Hashimoto D, Yan X, Helft J, Park PJ, Ma G, et al. R-Ras is required for murine dendritic cell maturation and CD4+ T-cell priming. *Blood*. 2012;119:1693–701.
- Wennstrom S, Downward J. Role of phosphoinositide 3-kinase in activation of ras and mitogen-activated protein kinase by epidermal growth factor. *Mol Cell Biol*. 1999;19:4279–88.
- Ritchie ME, Phipson B, Wu D, Hu Y, Law CW, Shi W, et al. limma powers differential expression analyses for RNA-sequencing and microarray studies. *Nucleic Acids Res*. 2015;43:e47.

34. Huang da W, Sherman BT, Lempicki RA. Bioinformatics enrichment tools: paths toward the comprehensive functional analysis of large gene lists. *Nucleic Acids Res.* 2009;37:1–13.
35. Huang-da W, Sherman BT, Lempicki RA. Systematic and integrative analysis of large gene lists using DAVID bioinformatics resources. *Nat Protoc.* 2009;4:44–57.
36. Subramanian A, Tamayo P, Mootha VK, Mukherjee S, Ebert BL, Gillette MA, et al. Gene set enrichment analysis: a knowledge-based approach for interpreting genome-wide expression profiles. *Proc Natl Acad Sci USA.* 2005;102:15545–50.
37. Reich M, Liefeld T, Gould J, Lerner J, Tamayo P, Mesirov JP. *GenePattern 2.0.* *Nat Genet.* 2006;38:500–1.

ACKNOWLEDGEMENTS

The XRB's project leading to these results has received funding from the Spanish Association against Cancer (GC16173472GARC), the Castilla-León government (CSI018P23), grants funded by MCIN/AEI/10.13039/501100011033/ plus the European Research Development Fund «A way of making Europe» of the European Union (PID2021-122666OB-I00, PDC2022-133027-I00, PLEC2022-009217), «la Caixa» Banking Foundation (HR20-00164), the «Programa Excelencia» of the Fundación Científica AECC 2022 (EPAEC222641CICS), and the «Escalera de Excelencia» of the Education Ministry of the Castilla y León autonomous government plus the European Research Development Fund (CLU-2023-2-01).

AUTHOR CONTRIBUTIONS

IF-P participated in all experimental work, analyzed data, and contributed to artwork design and manuscript writing. LFL-M carried out *in silico* analyses. MD and MB provided experimental reagents and contributed to both data analysis and manuscript writing. ES provided experimental reagents and analyzed data. B.A. contributed with mouse models and data analysis. XRB conceived the work, analyzed data, wrote the manuscript, and carried out the final editing of figures.

COMPETING INTERESTS

The authors declare no competing interests.

ADDITIONAL INFORMATION

Supplementary information The online version contains supplementary material available at <https://doi.org/10.1038/s41388-025-03367-3>.

Correspondence and requests for materials should be addressed to Xosé R. Bustelo.

Reprints and permission information is available at <http://www.nature.com/reprints>

Publisher's note Springer Nature remains neutral with regard to jurisdictional claims in published maps and institutional affiliations.



Open Access This article is licensed under a Creative Commons Attribution-NonCommercial-NoDerivatives 4.0 International License, which permits any non-commercial use, sharing, distribution and reproduction in any medium or format, as long as you give appropriate credit to the original author(s) and the source, provide a link to the Creative Commons licence, and indicate if you modified the licensed material. You do not have permission under this licence to share adapted material derived from this article or parts of it. The images or other third party material in this article are included in the article's Creative Commons licence, unless indicated otherwise in a credit line to the material. If material is not included in the article's Creative Commons licence and your intended use is not permitted by statutory regulation or exceeds the permitted use, you will need to obtain permission directly from the copyright holder. To view a copy of this licence, visit <http://creativecommons.org/licenses/by-nc-nd/4.0/>.

© The Author(s) 2025